Calcium Feedback and Sensitivity Regulation in Primate Rods

T. TAMURA, K. NAKATANI, and K.-W. YAU

From the Howard Hughes Medical Institute and Department of Neuroscience, The Johns Hopkins University School of Medicine, Baltimore, Maryland 21205

ABSTRACT Membrane current was recorded from a single primate rod with a suction pipette while the cell was bath perfused with solutions maintained at a temperature of ~38°C. A transient inward current was observed at the onset of bright illumination after briefly exposing the outer segment in darkness to Ringer's (Locke) solution containing 3-isobutyl-1-methylxanthine (IBMX), an inhibitor of cGMP phosphodiesterase. After briefly removing external Na^+ from around the outer segment in darkness, a similar current was observed upon Na^+ restoration in bright light. By analogy to amphibian rods, this inward current was interpreted to represent the activity of an electrogenic Na^+-dependent Ca^{2+} efflux, which under physiological conditions in the light is expected to reduce the free Ca^{2+} in the outer segment and provide negative feedback (the "Ca^{2+} feedback") to the phototransduction process. The exchange current had a saturated amplitude of up to ~5 pA and a decline time course that appeared to have more than one exponential component. In the absence of the Ca^{2+} feedback, made possible by removing the Ca^{2+} influx and efflux at the outer segment using a 0 Na^+–0 Ca^{2+} external solution, the response of a rod to a dim flash was two to three times larger and had a longer time to peak than in physiological solution. These changes can be approximately accounted for by a simple model describing the Ca^{2+} feedback in primate rods. The dark hydrolytic rate for cGMP was estimated to be 1.2 s^{-1}. The incremental hydrolytic rate, $\beta^*(t)$, activated by one photoisomerization was ~0.09 s^{-1} at its peak, with a time-integrated activity, $\int\beta^*(t)dt$, of ~0.033, both numbers being derived assuming spatial homogeneity in the outer segment. Finally, we have found that primate rods adapt to light in much the same way as amphibian and other mammalian rods, such as showing a Weber-Fechner relation between flash sensitivity and background light. The Ca^{2+} feedback model we have constructed can also explain this feature reasonably well.

INTRODUCTION

Phototransduction in retinal rods is now known to involve a light-stimulated biochemical cascade that eventually leads to the activation of a cGMP phosphodi-

Address reprint requests to Dr. King-Wai Yau, Department of Neuroscience, The Johns Hopkins University, School of Medicine, 725 N. Wolfe Street, Baltimore, MD 21205.

Dr. Tamura's present address is Department of Ophthalmology, Kanazawa University School of Medicine, 13-1 Takara-machi, Kanazawa, Ishikawa 920, Japan.

J. GEN. PHYSIOL. © The Rockefeller University Press · 0022-1295/91/07/0095/36 $2.00
Volume 98 July 1991 95–130

esterase, whence a reduction in free cGMP level in the outer segment of the cells (see, for example, Pugh and Cobbs, 1986; Stryer, 1986, for review). This decrease in cGMP in turn closes a cGMP-activated conductance (the "light-regulated" conductance) that sustains an inward current in darkness (see Yau and Baylor, 1989, for review); as a result, a membrane hyperpolarization is produced as the transduced neural signal.

In amphibian rods, the inward dark current through the light-regulated conductance is now known to be partly carried by Ca^{2+} (Yau and Nakatani, 1984*a*, 1985*a;* Hodgkin et al., 1985; Nakatani and Yau, 1988*a*). This dark Ca^{2+} influx is balanced by an equal efflux through a Na^+–Ca^{2+} exchange carrier at the outer segment (Yau and Nakatani, 1985*a;* Nakatani and Yau, 1988*a;* see also Schnetkamp, 1986; Hodgkin et al., 1987; Hodgkin and Nunn, 1987; Lagnado et al., 1988; Cervetto et al., 1989). Illumination reduces or stops the Ca^{2+} influx without affecting the efflux, thus causing the internal free Ca^{2+} concentration to decrease (Yau and Nakatani, 1985*a;* Gold, 1986; McNaughton et al., 1986; Miller and Korenbrot, 1987; Nakatani and Yau, 1988*a;* Ratto et al., 1988). This decrease in free Ca^{2+} provides a negative feedback that has been shown to influence the absolute sensitivity of a rod to light, as well as being important in light adaptation (Yau and Nakatani, 1985*a;* Korenbrot and Miller, 1986; Torre et al., 1986; Yau et al., 1986; Matthews et al., 1988; Nakatani and Yau, 1988*a, b,* 1989; Fain et al., 1989). The mechanism underlying this Ca^{2+} feedback seems to arise from a negative modulation of Ca^{2+} on the guanylate cyclase enzyme, which synthesizes cGMP (see, for example, Lolley and Racz, 1982; Pepe et al., 1986; Hodgkin and Nunn, 1988; Koch and Stryer, 1988; Rispoli et al., 1988; Kawamura and Murakami, 1989).

Relatively little is known about the details of the phototransduction mechanism in mammalian rods, though a qualitatively similar picture is expected to apply. Several years ago, however, it was reported that primate rods, unlike amphibian rods, show little sign of light adaptation (Baylor et al., 1984). This raised the possibility of a difference in physiological behavior between amphibian and mammalian rods. We have examined this question more closely by studying rod cells from a variety of mammalian species, but found this not to be the case. The experiments on several nonprimate mammalian species are already published (Tamura et al., 1989; Nakatani et al., 1991). In this paper we describe the experiments on primate rods. We begin with a study of the Na^+-dependent Ca^{2+} efflux, as well as the effect of the resulting Ca^{2+} feedback on the absolute flash sensitivity of these cells. We then show that these cells adapt to background light much like amphibian and other mammalian rods. Finally, we show that a simple model of the Ca^{2+} feedback is able to explain this light adaptation reasonably well.

A preliminary report of some of these results has appeared (Nakatani et al., 1990).

METHODS

Retinal Preparation

Most experiments were done on retinal rods from the cynomolgus (*Macaca fascicularis*) and the rhesus (*Macaca mulatta*) monkeys. For background light adaptation experiments, retinal rods from the green monkey (*Cercopithecus aethiops*) and the nocturnal bush baby (*Galago garnetti*) were also used. The first three species were kept in the animal quarters of the Division of

Comparative Medicine at Johns Hopkins School of Medicine, while the bush baby was flown in from the Duke University Primate Facility (Durham, NC) and used immediately. In all cases, the animal was dark-adapted for an hour, then sedated with an intramuscular injection of ketamine (10–15 mg/kg) before being put under general anaesthesia with sodium pentobarbital (10–15 mg/kg i.v.). One or both eyes were then removed in dim red light, after which the animal was killed by an overdose of pentobarbital (60 mg/kg i.v.) and then turned over to another laboratory for use of other body tissues. All subsequent procedures on the eye were performed in infrared light. An eye was coronally hemisected and under Locke solution (see below) many small pieces of peripheral retina were removed from the posterior eyecup. The retinal pieces were kept in oxygenated DMEM or L-15 culture medium (Gibco Laboratories, Grand Island, NY) in a light-tight container in the cold, and used over a period of ~36 h. During storage of the retinal pieces, the culture medium was in many instances continuously and gently stirred on a rotating platform while being bubbled with O_2 or O_2/CO_2. No obvious difference in the physiology of the rods was found with and without this step. When needed, a piece of retina was treated for 20–25 min with 100 U/ml collagenase (CLSPA grade; Worthington Biochemical Corp., Freehold, NJ) and 0.3 mg/ml hyaluronidase (type IV; Sigma Chemical Co., St. Louis, MO) in Locke solution to remove the extracellular matrix (see Baylor et al., 1984; Nakatani et al., 1991), then washed twice in Locke solution. Afterward, it was placed receptor-side up on cured Sylgard in a small petri dish containing Locke solution, and chopped finely with a razor blade. The chopped retinal pieces were transferred into the experimental chamber with a micropipette. For experiments on dissociated rods, the retinal piece was treated for 15 min with papain (Worthington Biochemical Corp.; at 10–20 U/ml and with 0.25 mg/ml L-cysteine as activator) instead of collagenase/hyaluronidase, then washed and chopped as before.

Recordings and Optics

The experiments described in this paper were similar in protocol to those already published for amphibian and nonprimate mammalian rods (Nakatani and Yau, 1988*a*, 1989; Nakatani et al., 1991). The technique consisted of recording membrane current from a rod photoreceptor by drawing either the inner or the outer segment of the cell into a snug-fitting glass pipette that was filled with Locke solution and connected to a current-to-voltage converter (see Yau et al., 1977; Baylor et al., 1979*a*; Lamb et al., 1981; Yau et al., 1981; Hodgkin et al., 1984). The position of the cell was adjusted so that the ciliary connection between the outer and inner segments was situated at the constriction of the pipette tip. Manipulations were made with the help of an infrared-sensitive TV camera system attached to the microscope. In the case of the rod outer segment within the pipette, the recorded cell was part of a fragment of retina. In the case of the inner segment within the pipette, dissociated rods were used. In this latter situation we had to choose dissociated cells with the cell body missing (i.e., left with the cylindrical inner and outer segments) in order to achieve good mechanical stability and high seal resistance during recording. Filled with Locke solution, the suction pipette typically had a resistance of 4–6 MΩ when empty and 10–20 MΩ with a cell in place. Assuming that the resistance of the empty electrode was equally distributed between its very tip and the shank, we calculated that ~80% of the membrane current should be recorded. Unless otherwise indicated, the values of the currents reported here have not been corrected for this incomplete current correction. In all of the figures, the membrane current is plotted with respect to the outer segment, so that a positive current corresponds to an outward membrane current at the outer segment. Low-pass filtering was used, with the high-frequency cutoff set at 20–100 Hz.

The optical bench design was similar to that described in Baylor et al. (1979*a*) and Lamb et al. (1981). Diffuse, unpolarized light at 500 nm was used throughout, with light incidence being approximately perpendicular to the longitudinal axis of the outer segment. Illumination

consisted of either brief flashes (8 ms duration) or steps of light. For *M. fascicularis, M. mulatta,* and *C. aethiops,* the rod outer segments were on average ~1.8 μm in diameter and 25 μm in length. Assuming an optical density of 0.016 μm^{-1} (Liebman, 1972; Harosi, 1975) and a quantum efficiency of 0.67 (Dartnall, 1972), an effective collecting area of ~0.8 μm^2 under our experimental conditions can be calculated (see Baylor et al., 1979*b*). For *G. garnetti,* the rod outer segments were of about the same length, but only ~1.2 μm in diameter, giving an effective collecting area of ~0.35 μm^2.

Perfusion Solutions and Temperature Control

For experiments in which an outer segment projecting from a small fragment of retina was inside the recording pipette (see above), bath perfusion was via a single solution inlet (method A) and could be switched between different solutions by a system consisting of two six-way rotary valves and a four-way slider valve as already described elsewhere (Nakatani and Yau, 1988*a*). Solution change around the tip of the pipette took ~300 ms to complete, as judged from junction current measurements (see Hodgkin et al., 1984). For experiments in which the inner segment of an isolated cell was drawn into the recording pipette, the outer segment could be subjected to more rapid solution changes via a theta tube inlet (see Hodgkin et al., 1985) connected directly to the two six-way rotary valves (method B). In this case, the chamber with the theta tube fixed to it was moved rapidly between two positions by combined electronic and

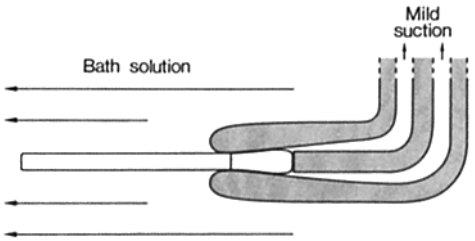

FIGURE 1. Recording configuration for an isolated primate rod.

pneumatic controls so that the recorded outer segment could be situated alternately in one or the other solution stream emerging from the two halves of the theta tubing. With this method, the solution change around the exposed outer segment could be achieved in <100 ms. To avoid bending and damage of the outer segment during perfusion, the tip of the suction pipette was bent at right angles to the main shank so that the long axis of the outer segment was oriented parallel to the solution stream. The rapid perfusion also had a tendency to draw the cell out of the pipette. To prevent this from happening, a small constant suction was applied inside the pipette so that the inner segment was rested against the end of a fine glass fiber appropriately positioned inside the pipette to serve as a "stop" (see Fig. 1).

For method A above, bicarbonate-buffered Locke solution (see Baylor et al., 1984) was used, containing (in mM): 120 NaCl, 3.6 KCl, 1.2 $CaCl_2$, 2.4 $MgCl_2$, 20 $NaHCO_3$, 0.02 Na-EDTA, 3 Na-HEPES, and 10 dextrose, pH 7.6. A separate solution containing, in addition, IBMX (3-isobutyl-1-methylxanthine) was also used when required (see Fig. 2*A*). The solution(s) was maintained at 38°C in a water bath and continuously bubbled with 95% O_2–5% CO_2. The solution cooled significantly during transit from the water bath to the experimental chamber, and was reheated by a heating coil just before entry into the chamber so that the temperature registered at the tip of the suction pipette was again 38°C. For method B above, HEPES-buffered Locke solution (see Baylor et al., 1984; Nakatani et al., 1991) was used, containing (in mM): 140 NaCl, 3.6 KCl, 1.2 $CaCl_2$, 2.4 $MgCl_2$, 0.02 Na-EDTA, 3 Na-HEPES, and 10 dextrose,

pH 7.6. Lithium and guanidinium Locke solutions contained, respectively, LiCl and guanidinium Cl instead of NaCl, and TMA (tetramethylammonium)-EDTA and TMA-HEPES instead of the Na^+-containing buffers. The 0 Na^+–0 Ca^{2+} solution used for eliminating the Ca^{2+} feedback (Nakatani and Yau, 1988*b*, 1989) consisted of either lithium or guanidinium Locke solution in which $CaCl_2$ was omitted and 0.2 mM TMA-EGTA was added. In this perfusion method, the solution at the water bath was maintained at 50–60°C, such that without any reheating during transit into the chamber the temperature would drop to ~38°C at the pipette tip. The difference in temperature between the solutions emerging from the two halves of the theta tubing was <1°C.

The temperature near the recorded cell was measured by a thermistor probe (YSI Instrument Co., Yellow Springs, OH) attached to the suction pipette, with the sensor of the probe situated within 0.5 mm behind the tip of the pipette (see Baylor et al., 1980; Nakatani et al., 1991).

The records shown in Figs. 2 *B*, 4, and 5 already had the junction currents resulting from solution changes removed by subtraction (see Nakatani and Yau, 1988*a*; also Hodgkin et al., 1984). The ramps in the solution trace of these figures indicate the approximate time courses of solution change, corresponding to the time durations required for ~90% completion of a junction current upon solution change.

RESULTS

Na^+-dependent Ca^{2+} Efflux

Since the Na^+-dependent Ca^{2+} efflux at the outer segment is known to be a key mechanism in sensitivity regulation and background light adaptation in amphibian rods, we sought to identify and characterize a similar efflux in primate rods. The steady dark Ca^{2+} efflux under physiological conditions is expected to be small because the experiments on amphibian rods have suggested that only 10–15% of the dark current through the light-regulated conductance is carried by Ca^{2+} (Yau and Nakatani, 1985*a*; Nakatani and Yau, 1988*a*). The smallness of the physiological Ca^{2+} efflux, together with its relatively rapid decline in the light (see below), imposes difficulties for its identity in Locke solution. One way to exaggerate this Ca^{2+} efflux for easier study is to increase the dark Ca^{2+} influx, such as with the drug IBMX, which is known to increase the dark conductance by raising the concentration of intracellular cGMP (Lipton et al., 1977; Capovilla et al., 1982; Cervetto and McNaughton, 1986). We have previously adopted this strategy in amphibian rods (Yau and Nakatani, 1985*a*; Nakatani and Yau, 1988*a*). The Ca^{2+} efflux can be measured as an electrical current, because the Na^+–Ca^{2+} exchange is electrogenic (Yau and Nakatani, 1984*b*; Cervetto et al., 1989).

Fig. 2 *A* shows such an experiment on a *M. mulatta* rod. Here a rod outer segment projecting from a fragment of retina was exposed to 0.5 mM IBMX in bath Locke solution for ~30 s before being drawn into the recording pipette and stimulated with a light step. The response of the cell did not immediately reach the zero-current level, but stayed briefly at a plateau of about −4 pA before gradually relaxing to zero. By analogy to amphibian experiments, this transient current is taken to represent an exaggerated electrogenic Na^+-dependent Ca^{2+} efflux due to the presence of IBMX. From a total of four experiments (one on *M. fascicularis* and three on *M. mulatta* rods), with IBMX exposure times of 8 s–2 min, the plateau of the exchange current ranged from 2.9 to 5.2 pA (mean ± SD = 4.0 ± 0.9 pA). We assume that the top end

of the current range, namely, 5.2 pA, is closer to what would be observed in the best of cell conditions. After correcting for the incomplete collection of current by the suction pipette (see Methods), this saturated amplitude of the exchange current would reach ~6.5 pA.

A variant of the above method is to expose the rod outer segment to IBMX in the

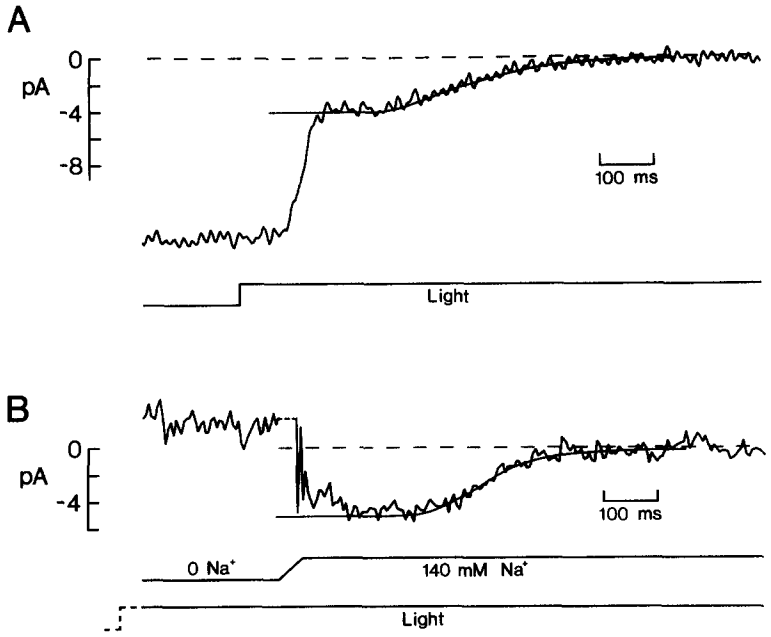

FIGURE 2. Na^+–Ca^{2+} exchange current measured from a single primate rod. (*A*) *M. mulatta* rod. An outer segment projecting from a retinal fragment was sucked into the recording pipette after being exposed to 0.5 mM IBMX in Locke solution for ~30 s. The exchange current was visible at the initial plateau of the response to a bright step of light (12,000 Rh* s^{-1}). Maximum exchange current was 3.9 pA. Sweep is from a single experimental trial. Cell 3 of Table I. 37.5°C. (*B*) *M. fascicularis* rod. Isolated cell, with the inner segment in the recording pipette. The outer segment was exposed to 0.2 mM IBMX in a 0 Na^+–140 guanidinium solution for 3 s to induce Ca^{2+} loading before the onset of the light step (3,400 Rh* s^{-1}). The exchange current was then activated by switching back to Locke solution. A few large spikes caused by mechanical vibration appeared during the solution change; in the figure these spikes have been removed and replaced by a small dashed line. Also, the junction current caused by solution change probably has not been completely subtracted out (see Methods) in this experiment, as indicated by the small shift in baseline. Sweep indicates the average of two trials. Cell 5 of Table I. 36.5°C. Bandwidth is DC-100 Hz in both experiments. See text for the curve fits.

absence of external Na^+, so that the dark Ca^{2+} influx can be trapped in the outer segment (see Yau and Nakatani, 1985*a;* Nakatani and Yau, 1988*a*, 1989). After a brief period in this Ca^{2+} loading solution, a large Ca^{2+} efflux can then be activated by restoring external Na^+. Fig. 2 *B* shows an experiment of this kind on a *M. fascicularis* rod. Before the beginning of the trace shown in the figure, the rod outer segment was

exposed to the loading solution (consisting of Locke solution with 0.2 mM IBMX and also guanidinium in place of Na^+) for only 3 s in darkness before bright light was turned on to suppress all dark current. Upon restoring external Na^+, a transient inward current again appeared, with a plateau amplitude of −4.8 pA. To permit rapid solution changes, this kind of experiment was performed on an isolated rod, with the inner segment inside the recording pipette and the outer segment exposed to perfusing solutions emerging from a theta tube (see Methods). Owing to difficulties in maintaining recording stability and in finding a suitable cell with sufficient dark current, however, the experiment in Fig. 2 *B* represents the only acceptable experiment of this kind.

The curve-fitting in either panel of Fig. 2 is done as follows. For Ca^{2+} efflux alone in bright light, we can write, from Eq. A3 in the Appendix:

$$\frac{dCa_T}{dt} = -\frac{j_{ex}}{FV} \tag{1}$$

where

$$j_{ex} = J_{ex}\left(\frac{Ca_f}{Ca_f + K_{ex}}\right) \tag{A6}$$

These equations describe a Ca^{2+} extrusion process that is governed by Michaelis binding. Ca_f and Ca_T are the internal free and "total exchangeable" (see Appendix) Ca^{2+} concentrations, respectively, K_{ex} is the Ca_f value that would half-saturate the Na^+–Ca^{2+} exchange, j_{ex} is the exchange current, J_{ex} is the saturated exchange current, F is Faraday's constant, and V is the cytosolic volume of the rod outer segment. Considering initially a single intracellular Ca^{2+} buffer, and assuming a rapid equilibrium between Ca^{2+} and the buffer, Ca_f and Ca_T are then related by (see Appendix):

$$Ca_T = Ca_f\left(1 + \frac{R_T}{Ca_f + K_D}\right) \tag{A2}$$

where R_T is the total buffer concentration and K_D is the dissociation constant.

We take the physiological j_{ex} and Ca_f of a typical primate rod in darkness to be 1 pA and 0.3 μM, respectively (see $j_{ex,0}$ and $Ca_{f,0}$ in the Appendix). We further take J_{ex} = 6.5 pA (see above). From Eq. A6, then, K_{ex} = 1.65 μM (cf. Cervetto et al., 1987). Finally, we assume that the cytosolic volume of the primate rod outer segment is half of total, which gives $V \simeq 30$ μm^3 for an outer segment of 1.8 μm in diameter and 25 μm in length (see Methods). With the given values of R_T and K_D, Eqs. 1, A2, and A6 can be solved numerically with the initial condition of an arbitrarily high Ca_T value. Appropriate R_T and K_D values are chosen by trial and error to give a time course of decline of the exchange current that best fits the data. As an example, the decline time course of the exchange current in Fig. 2 *A* is replotted on semi-logarithmic coordinates in Fig. 3 (filled circles). The dashed curve in Fig. 3 shows the predicted decline time course with R_T = 400 μM and K_D = 3 μM; vertical and horizontal adjustments of the curve have been made so that its form can be compared with the data. Analysis of all five cells gave average best-fit R_T and K_D values of 360 ± 40 (SD) and 3 ± 0.7 μM, respectively. The final exponential decline time constant for the exchange current calculated from these average R_T and K_D values would be ~90 ms.

The above assumption of a single Ca^{2+} buffer has the attraction that there are only two free parameters, R_T and K_D, to be considered. In actuality, however, the final decline of the exchange current most probably contains more than one exponential component, as indicated by the curvature of the observed decline time course at small current amplitudes in Fig. 3. This curvature, while small (having been exaggerated by the logarithmic plot of Fig. 3), was observed in all five experiments. The observed decline time course can be better described with a two-buffer system (see also Hodgkin et al., 1987). In this case, Eq. A2 has to be replaced by the following equation:

$$Ca_T = Ca_f\left(1 + \frac{R_{T,1}}{Ca_f + K_{D,1}} + \frac{R_{T,2}}{Ca_f + K_{D,2}}\right) \tag{2}$$

where subscripts 1 and 2 refer to the two buffer systems. The solid curve in Fig. 3, which fits the data better than the dashed curve, is drawn using $R_{T,1}$ = 400 μM, $K_{D,1}$ = 3 μM, $R_{T,2}$ = 85 μM, and $K_{D,2}$ = 0.05 μM. This curve is drawn in linear coordinates in Fig. 2 *A*. A curve of near-identical shape (not shown) can also be generated when rapid equilibrium between Ca^{2+} and its buffers is not assumed (that is, the buffers are relatively "slow"). In this case, Eqs. 1 and 2 have to be replaced by:

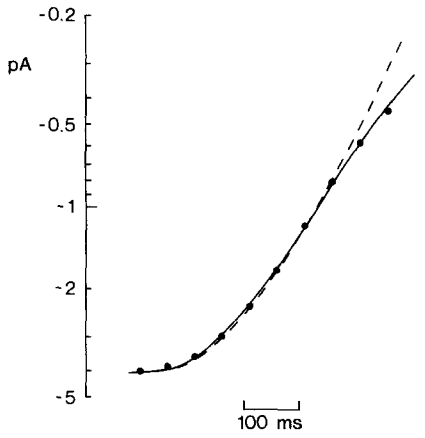

FIGURE 3. Decline time course of the exchange current from Fig. 2 *A* replotted on semi-logarithmic coordinates. The current amplitude is indicated at 50-ms intervals by filled circles. The dashed curve is drawn on the assumption of a single intracellular Ca^{2+} buffer, according to Eqs. 1, A2, and A6. The continuous curve is drawn on the assumption of two intracellular buffers, according to Eqs. 1, 2, and A6. See text for details and the chosen values of the various parameters. The positions of both curves have been adjusted vertically to coincide with the data points at plateau level.

$$\frac{dCa_f}{dt} = -\left(\frac{1}{FV}\right)j_{ex} - \frac{dCa_{b,1}}{dt} - \frac{dCa_{b,2}}{dt} \tag{3}$$

$$\frac{dCa_{b,1}}{dt} = k_{on,1}Ca_f(R_{T,1} - Ca_{b,1}) - k_{off,1}Ca_{b,1} \tag{4}$$

$$\frac{dCa_{b,2}}{dt} = k_{on,2}Ca_f(R_{T,2} - Ca_{b,2}) - k_{off,2}Ca_{b,2} \tag{5}$$

where the various k's represent binding and unbinding rates for the two buffers. Eqs. 4 and 5 are merely rewritten from Eq. A1 in the Appendix. The appropriate

parameters to fit the data in Fig. 3 are $R_{T,1}$ = 450 μM, $K_{D,1} \equiv k_{off,1}/k_{on,1}$ = 8 μM, $k_{off,1}$ = 20 s^{-1}, $R_{T,2}$ = 90 μM, $K_{D,2} \equiv k_{off,2}/k_{on,2}$ = 0.5 μM, $k_{off,2}$ = 5 s^{-1}. The values of $k_{off,1}$ and $k_{off,2}$ are somewhat arbitrary, with the only selection criterion being that these rates are low enough so that oscillations are not obvious in the computed flash and step responses (see later). The values for fitting each of the five experiments using two rapid or slow buffers are collected in sections *A* and *B* of Table I, and the average values are used for modeling later on. The experiment in Fig. 2 *B* corresponds to cell 5 in Table I. Even though slow Ca^{2+} buffering involves additional parameters, in

TABLE I

Collected Curve-Fitting Parameters for the Decline Time Course of the Exchange Current

A. Two fast buffers (i.e., rapid equilibrium): C_0 = 0, K_{ex} = 1.65 μM

Cell	$R_{T,1}$	$K_{D,1}$	$R_{T,2}$	$K_{D,2}$
	μ*M*	μ*M*	μ*M*	μ*M*
1	370	4.2	95	0.06
2	350	2.6	100	0.07
3	400	3.0	85	0.05
4	350	3.2	75	0.07
5	300	4.0	80	0.05
Mean	354	3.4	87	0.06
SD	36.5	0.68	10.4	0.01

B. Two slow buffers: C_0 = 0, K_{ex} = 1.65 μM, $k_{off,1}$ = 20 s^{-1}, $k_{off,2}$ = 5 s^{-1}

Cell	$R_{T,1}$	$K_{D,1}$	$R_{T,2}$	$K_{D,2}$
	μ*M*	μ*M*	μ*M*	μ*M*
1	650	30	100	0.50
2	400	9.0	110	0.50
3	450	8.0	90	0.50
4	450	12	85	0.55
5	600	50	90	0.50
Mean	510	21.8	95	0.51
SD	108	18.1	10	0.022

C. Two slow buffers: C_0 = 0.1 μM, K_{ex} = 1.1 μM, $k_{off,1}$ = 20 s^{-1}, $k_{off,2}$ = 5 s^{-1}

Cell	$R_{T,1}$	$K_{D,1}$	$R_{T,2}$	$K_{D,2}$
	μ*M*	μ*M*	μ*M*	μ*M*
1	650	23	140	0.30
2	400	6.1	150	0.40
3	450	6.0	140	0.25
4	450	8.0	115	0.40
5	600	35	110	0.30
Mean	510	15.6	131	0.33
SD	108	13.0	17.5	0.067

C_0 refers to the constant in Eq. 19. In *A* and *B*, with C_0 = 0, Eq. 19 reduces to Eq. A6. In *C*, the value of 1.1 μM for K_{ex} is obtained from Eq. 19 with $j_{ex,0}$ = 1 pA and $J_{ex,0}$ = 6.5 pA. See text for details.

subsequent modeling it gives flash and step responses that resemble observations a little more (see Figs. 6 and 10). Finally, Table I, part *C*, gives the curve-fitting parameters for a more elaborate situation in which Eq. A6 is replaced by Eq. 19, to be described later.

Influence of the Ca^{2+} Feedback on Light Sensitivity

Since a Na^+-dependent Ca^{2+} efflux exists in primate rods, it is natural to ask whether it influences the light sensitivity of these cells via a Ca^{2+} feedback, as in amphibian rods (see Introduction). This question can be answered by removing the putative Ca^{2+} feedback from a primate rod and noting any change in the response of the cell to a dim flash compared with control (Nakatani and Yau, 1989). Fig. 4 shows such an

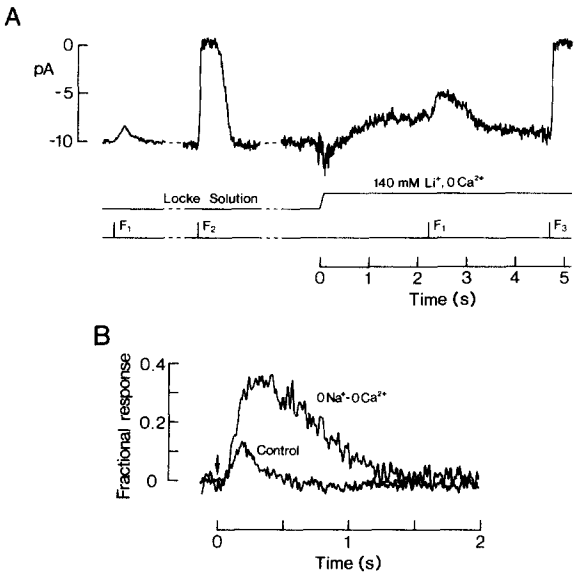

FIGURE 4. Effect of removing the Ca^{2+} feedback on dim flash sensitivity. Isolated *M. mulatta* rod, with the inner segment within the recording pipette. (*A*) A dim flash and a bright flash were delivered to measure light sensitivity and dark current amplitude in both Locke solution and a 0 Na–0 Ca solution (which removes the feedback). Sweep in Li solution represents the average of two trials, while the dim- and bright-flash responses in Locke solution represent the average of eight and two trials, respectively. The flashes F_1, F_2, and F_3 delivered 9.8, 280, and 370 Rh*, respectively. DC-40 Hz, 37°C. (*B*) Comparison of the dim-flash responses in the two solutions shown in *A*. Arrow indicates timing of the flash. Both responses are already normalized against the respective dark currents; for this purpose, the slow drift of the dark current in the 0 Na–0 Ca solution has been corrected for by a linear-trend removal. Cell 4 of Table II.

experiment on a *M. mulatta* rod, using an isolated rod with the outer segment exposed to bath perfusion. In Fig. 4 *A*, the solution around the outer segment of the cell was rapidly switched at time zero to a 0 Na^+–0 Ca^{2+} Locke solution (see Methods), designed to remove the feedback by eliminating the Ca^{2+} influx and efflux simultaneously (Matthews et al., 1988; Nakatani and Yau, 1988*b*, 1989). Since the dark current is very sensitive to internal Ca^{2+}, its reasonable stability for the 5 s or so in this test solution suggested that the Ca^{2+} concentration probably did not change much during this period of time. A dim flash was delivered while the outer segment was in the 0 Na^+–0 Ca^{2+} solution to test for light sensitivity; a bright flash was also given to confirm the zero-current level. Exactly the same protocol was repeated once more to produce the average trace shown in the figure. Shown on the left-hand side is

the averaged response of the cell to an identical dim flash in control Locke solution, as well as the response to a bright flash, the amplitude of which gave the control dark current. The responses to the dim flash in both conditions are superposed in Fig. 4 *B*, with their amplitudes already normalized against the respective dark currents. The response in the absence of Ca^{2+} feedback is ~2.5 times (ignoring nonlinearities) larger than the control response, and the time to peak is about twice as long. Thus, the Ca^{2+} feedback indeed has an influence on the absolute sensitivity of primate rods to light. From a total of five experiments (three on *M. fascicularis* and two on *M. mulatta* rods; see also Fig. 6), the average increase in amplitude of the dim flash response was ~2.3-fold and the average time to peak increase was ~1.8-fold in the absence of Ca^{2+} feedback. Owing to the gradual run-down in the condition of the cell usually observed in this kind of experiment (presumably because of the inability of the cell to extrude the cation that replaced external Na^+), it was generally not possible to obtain more than several dim flash responses in the 0 Na^+–0 Ca^{2+} solution for averaging in a given experiment. Thus, the comparison between the light responses in the two conditions should be regarded as only approximate. Nonetheless, the quantitative changes seen here are broadly similar to those previously observed in amphibian rods and cones (Nakatani and Yau, 1989).

Metabolic Flux of cGMP in Darkness

We shall, in the next section, make an attempt to reproduce the effect of the Ca^{2+} feedback on the dim-flash response based on simple modeling. To achieve this, one necessary piece of information is the basal metabolic flux of cGMP in darkness. This basal flux rate can be estimated from the rate at which the dark current declines when cGMP synthesis is essentially stopped, a strategy first used by Hodgkin and Nunn (1988) on amphibian rods. The idea is that since the inhibition of the guanylate cyclase enzyme by Ca^{2+} shows a steep dependence on Ca^{2+} concentration (see Koch and Stryer, 1988; Kawamura and Murakami, 1989; also Eq. A9 in the Appendix here), any significant rise in internal Ca^{2+} will quickly reduce the cyclase activity to a very low level. This condition is realized, for instance, when the Na^+-dependent Ca^{2+} efflux is stopped in darkness by removal of external Na^+. From Eq. A12 in the Appendix, the cGMP concentration will change under these circumstances according to:

$$dG/dt = \alpha' - \beta_0 G \tag{6}$$

where G is cGMP concentration, α' is the low residual rate of cyclase activity at high Ca^{2+} concentration, and β_0 is the rate of dark phosphodiesterase activity. In practice, we found α' to be very small, in that the residual dark current was near zero (see, for example, Fig. 5), so that we can set $\alpha' \sim 0$. Eq. 6 then becomes:

$$dG/dt = -\beta_0 G \tag{7}$$

The gating of the conductance is described by Eq. A5 in the Appendix:

$$j_{ch} = (J_{ch}/K_{ch}^n)G^n \tag{A5}$$

or

$$dj_{ch}/dt = n(J_{ch}/K_{ch}^n)G^{n-1}dG/dt \tag{8}$$

Substituting Eqs. A5 and 8 in Eq. 7, we get:

$$dj_{ch}/dt = -n\beta_0 j_{ch} \tag{9}$$

which shows an exponential decline of j_{ch} with time, with a time constant τ_0 given by:

$$\tau_0 = 1/n\beta_0 \tag{10}$$

or

$$\beta_0 = 1/n\tau_0 \tag{11}$$

Fig. 5 shows such an experiment on a *M. fascicularis* rod. An isolated rod was again used, with the inner segment inside the recording pipette and the outer segment exposed to perfusion. Upon replacing external Na^+ with guanidinium, there was an initial reduction in dark current that was coincident with Na^+ removal, reflecting the different permeabilities of the conductance to Na^+ and guanidinium (see Nakatani and Yau, 1988*a*). Thereafter, however, the dark current declined approximately exponentially with a time constant of ~480 ms (indicated by the smooth curve). In

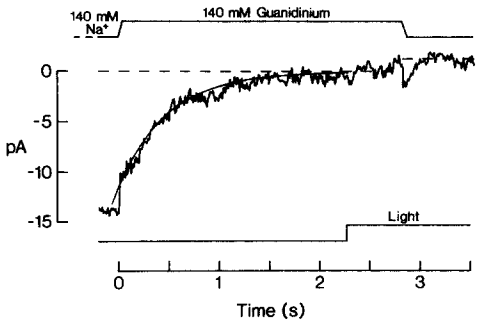

FIGURE 5. Decline time course of the dark current upon removing external Na^+. Isolated *M. fascicularis* rod, with the inner segment in the pipette. The slight shift in baseline upon restoring Na^+ is due to an incomplete removal of the junction current. Smooth curve is an exponential decline with time constant 480 ms. Sweep is average of two trials. Light step delivered 12,000 Rh* s^{-1}. DC-50 Hz, 38°C.

this experiment, the dark current seemed to reach a very small but non-zero steady level in guanidinium solution, as indicated by the tiny light response that could still be elicited by the bright light step. However, in four other experiments (three with guanidinium and one with Li^+ as the substitute for external Na^+) this residual current was practically nonexistent because no obvious light response was visible. The average τ_0 value from all of the experiments was 345 ± 80 ms. From Eq. 11, this gives a β_0 value of 1.2 s^{-1} for $n = 2.5$ (see Appendix).

Note that upon restoring external Na^+ in the light, a small transient current in the inward direction appeared (together with a slight shift in the baseline that was probably due to an incomplete subtraction of the junction current; see Methods). This transient current reflected the electrogenic Na^+–Ca^{2+} exchange activity that pumped out the Ca^{2+} trapped in the outer segment in darkness (see Yau and Nakatani, 1984*b*, 1985*a*; Nakatani and Yau, 1988*a*, 1989). By integrating this current over time, we obtained a total charge transfer of 0.32 pC. Since one net positive charge enters the cell via the exchange for each Ca^{2+} leaving (Yau and Nakatani, 1984*b*), the total Ca^{2+} efflux was $2 \times 0.32 = 0.64$ pC. This charge should correspond

approximately to the Ca^{2+} influx during the loading period in darkness. Dividing this influx by the total charge influx through the conductance (i.e., the area under the exponentially declining dark current while in guanidinium solution, ~5 pC) gives a fractional Ca^{2+} current of 0.13. After correcting for the apparent permeability ratio between guanidinium and Na^+, obtained by taking the ratio of the dark currents immediately before and after the removal of Na^+ (and ignoring the small contribution by the exchange current to the total measured dark current in the Na^+ solution), the fractional dark current carried by Ca^{2+} in Locke solution becomes ~0.10. This number is quite similar to what we previously measured in amphibian rods, which is 0.1–0.15 (Yau and Nakatani, 1985*a;* Nakatani and Yau, 1988*a*). In the other four experiments, the recordings immediately after Na^+ restoration were too noisy to give reliable estimates of the small Na^+–Ca^{2+} exchange current.

Modeling of Ca^{2+} Feedback on the Dim Flash Response

In this section we shall examine whether we can quantitatively predict the action of the Ca^{2+} feedback on the dim flash response of primate rods with a simple model. We assume that the Ca^{2+} feedback acts exclusively via a negative modulation of the guanylate cyclase enzyme by Ca^{2+}.

To proceed, we first need to derive the time course of the phosphodiesterase activity induced by a dim flash. Under the simplified experimental condition where the internal free Ca^{2+} concentration stays unchanged (i.e., in the absence of any Ca^{2+} feedback) Eq. A14 in the Appendix reduces to:

$$\frac{dG}{dt} = \beta_0 G_0 - [\beta_0 - \beta^*(t) I_F] G \tag{12}$$

where $\beta^*(t)$ is the rate of phosphodiesterase activity induced by one photoisomerization (Rh*) and I_F is the intensity of a dim flash. By change of variable from G to j_{ch} in Eq. 12 using Eqs. A5 and 8, we obtain, after rearranging terms:

$$\beta^*(t) I_F = \beta_0 [(j_{ch}/j_{ch,0})^{-1/n} - 1] - \frac{1}{n} j_{ch}^{-1} (dj_{ch}/dt) \tag{13}$$

where $j_{ch,0}$ is the dark current. Again, adopting $n = 2.5$ (see Appendix) and defining the normalized variable $\hat{j}_{ch} \equiv j_{ch}/j_{ch,0}$, we get:

$$\beta^*(t) I_F = \beta_0 (\hat{j}_{ch}^{-1/2.5} - 1) - \frac{1}{2.5} \hat{j}_{ch}^{-1} (d\hat{j}_{ch}/dt) \tag{14}$$

The analysis and modeling are shown in Fig. 6. Panel *A* shows the same kind of experiment as in Fig. 4, in which the response of a *M. fascicularis* rod to a dim flash in control Locke solution (trace *b*) was compared with that to an identical flash in a 0 Na^+–0 Ca^{2+} solution that removed the Ca^{2+} feedback (trace *a*). The amplitudes of the dim flash responses have again been plotted on a scale of normalized current. After smoothing trace *a* by a moving average of adjacent data points (over a time window of 70 ms) and then applying Eq. 14 with $\beta_0 = 1.2\ s^{-1}$ (the average value from the previous section), we obtained the time course of phosphodiesterase activity, $\beta^*(t) I_F$, triggered by the flash. This time course is indicated by the noisy trace in Fig. 6 *B*. It

reaches peak at ~0.2 s, and has a shape that closely parallels the electrical response in control solution. The calibrated I_F value in this experiment is 10 Rh*; thus, the peak value of $\beta^*(t)$ is ~0.1 s^{-1} Rh^{*-1}. We have fitted to the deduced time course of $\beta^*(t)$ a waveform corresponding to the convolution of three delay stages. We have

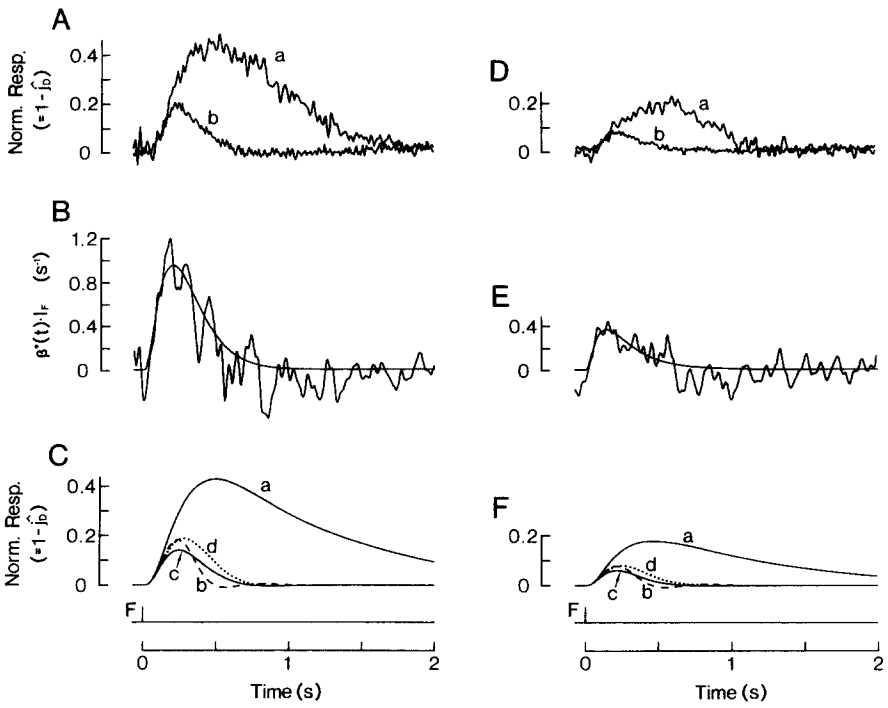

FIGURE 6. (*Top panels*) Same kind of experiment as in Fig. 4, from two other cells. Trace *a* shows the response to a dim flash in a 0 Na–0 Ca solution, and trace *b* shows the response to an identical flash in control Locke solution. Both responses are already normalized against the dark currents in the respective conditions. Flash (*F*) was delivered at time zero. (Left column) *M. fascicularis* rod. External Na^+ was replaced by guanidinium. Traces *a* and *b* represent averages of four and eight flash trials, respectively. Flash intensity was 9.8 Rh*. 36–38°C. (*Right column*) *M. mulatta* rod. Na^+ replaced by Li^+. Trace *a* was from a single flash trial, and trace *b* was the average of 15 trials. Flash intensity was 5.2 Rh*, 36.5°C. DC-40 Hz in both cases. (*Middle panels*) Time course of the flash-triggered phosphodiesterase activity, $\beta^*(t)I_F$, extracted from trace *a*. See text for details. Smooth curve is drawn from the convolution of exponential time constants 0.1, 0.1, and 0.1 s in *B* and 0.045, 0.045, and 0.2 s in *E*. See cells 1 and 5 in Table II for other information on these two experiments. (*Bottom panels*) Flash responses computed from $\beta^*(t)I_F$ in middle panels. Trace *a* is computed in the absence of Ca^{2+} feedback; traces *b–d* are all computed with the feedback imposed, but are different in details (see text).

adopted three delay stages because they have correlates in the biochemistry underlying phototransduction. Thus, a photon is known to photoisomerize a rhodopsin molecule, which in turn activates many G protein (transducin) molecules; each of these G protein molecules then activates a cGMP phosphodiesterase molecule (see,

for example, Pugh and Cobbs, 1986; Stryer, 1986). On this basis, the three delay stages can be interpreted to represent the decay time courses of the active pigment molecule, the active G protein, and the active phosphodiesterase, respectively (Nakatani and Yau, 1989). It should be emphasized, however, that in principle the computations carried out below do not require a mathematical expression for $\beta^*(t)$ that is biologically accurate, as long as it describes the time course of $\beta^*(t)$ deduced from data. For Fig. 6 *B*, we found that three delay stages each of 0.1 s time constant can fit the activated phosphodiesterase time course fairly well (smooth curve). Applying the fitted function for $\beta^*(t)I_F$ back to Eqs. 12 and A5 produces trace *a* in Fig. 6 *C*, which is fairly similar to trace *a* in Fig. 6 *A*, as would be expected since the latter is the starting point of the analysis. The derived $\beta^*(t)$ shows a hint of a slight undershoot, a consistent finding in all five experiments (see also Fig. 6 *E*). It is not certain, however, whether this is genuine or merely represents an artifact arising from, say, an incomplete clamping of the Ca^{2+} concentration in the 0 Na^+–0 Ca^{2+} solution. In the curve-fitting of $\beta^*(t)$ we have ignored this mild undershoot, which probably explains the slight difference between trace *a* in Fig. 6 *A* and trace *a* in Fig. 6 *C*.

A closely related method for measuring $\beta^*(t)$ has also been described by Hodgkin and Nunn (1988). This method involves removing external Na^+, as shown in Fig. 5, at various time instants during the electrical response to a flash. Both this method and the one we used should lead to the same $\beta^*(t)$, but our method is simpler to carry out experimentally, especially for the fragile primate rods, because it does not involve repeated solution changes.

With $\beta^*(t)I_F$ in hand, the Ca^{2+} feedback can now be imposed to generate the electrical response to the same dim flash under physiological conditions. In the case of two fast Ca^{2+} buffers (that is, assuming rapid equilibrium between Ca^{2+} and the buffers), the appropriate equations are Eq. 2 and (see Appendix):

$$\frac{dCa_T}{dt} = \left(\frac{1}{FV}\right)\left[0.05\left(\frac{J_{ch}}{K_{ch}^n}\right)G^n - J_{ex}\left(\frac{Ca_f}{Ca_f + K_{ex}}\right)\right] \tag{A7}$$

$$\frac{dG}{dt} = \beta_0 G_0\left[\frac{1 + (Ca_{f,0}/K_{cy})^m}{1 + (Ca_f/K_{cy})^m}\right] - [\beta_0 + \beta^*(t)I_F]G \tag{A14}$$

$$j_D = j_{ch} + j_{ex} \tag{A15}$$

Eq. A7 describes the influx and efflux of Ca^{2+}. Eq. A14 describes the cGMP metabolism and its modulation by internal Ca^{2+}. Finally, Eq. A15 simply states that the total measured dark current represents the sum of the inward current through the conductance and the net inward current through the Na^+–Ca^{2+} exchange. The Ca^{2+} buffering parameters are given by the average values in Table I, part *A*. We also used J_{ex} = 6.5 pA, K_{ex} = 1.65 μM, V = 30 μm^3, β_0 = 1.2 s^{-1} (see above), K_{ch} = 50 μM, K_{cy} = 0.1 μM, m = 4, and n = 2.5 (see Appendix). For initial conditions, we use $Ca_{f,0}$ = 0.3 μM, G_0 = 7.9 μM, $j_{ch,0}$ = 20 pA, $j_{ex,0}$ = 1 pA, $j_{D,0} = j_{ch,0} + j_{ex,0}$ = 21 pA (see Appendix). Trace *b* (dashed) in Fig. 6 *C* shows the computed physiological response in normalized form. It is similar in both amplitude and time to peak to trace *b* in Fig. 6 *A*, which is the physiological response actually recorded. A hint of oscillations,

common for a negative feedback system, is present in the falling phase of the computed response; this is not obvious in the recorded response (but see Discussion).

Computations can also be carried out for the situation of two slow buffers. In this case, the equations are Eqs. 4, 5, A14, A15, and the following:

$$\frac{d[Ca_f]}{dt} = -\left(\frac{1}{FV}\right)\left[0.05\left(\frac{J_{ch}}{K_{ch}^n}\right)G^n - J_{ex}\left(\frac{[Ca_f]}{[Ca_f] + K_{ex}}\right)\right] - \frac{d[Ca_{b,1}]}{dt} - \frac{d[Ca_{b,2}]}{dt} \quad (15)$$

The average values in Table I, part B are used for specifying the Ca^{2+} buffering. The derived waveform is indicated by trace *c* (solid) in Fig. 6 *C*. This waveform resembles the observed response a little more, with less conspicuous oscillations. Trace *d* will be described below.

Fig. 6, *D–F*, show another experiment, on a *M. mulatta* rod, analyzed in the same manner and with similar results. In this case, the smooth waveform in Fig. 6 *E* is

TABLE II

Collected Parameters for $\beta^*(t)$

Cell	τ_1	τ_2	τ_3	t_{peak}	β^*_{peak}	$\int\beta^*(t)dt$
	s	*s*	*s*	*s*	$Rh^{*-1}s^{-1}$	Rh^{*-1}
1	0.1	0.1	0.1	0.20	0.098	0.036
2	0.1	0.1	0.1	0.20	0.047	0.017
3	0.135	0.135	0.135	0.27	0.120	0.060
4	0.08	0.08	0.08	0.16	0.091	0.027
5	0.045	0.045	0.2	0.15	0.070	0.026
Mean				0.20	0.085	0.033
SD				0.05	0.028	0.016

τ_1, τ_2, and τ_3 are the three exponential time constants used to fit the waveform of $\beta^*(t)$ by convolution. The variations in these fitted time constants among different cells should not be taken too literally because they are quite sensitive to the shape of the derived $\beta^*(t)$, which is only approximate. t_{peak} is the time to peak of $\beta^*(t)$. β^*_{peak} is the value of $\beta^*(t)$ at t_{peak}. These five cells are not the same as those in Table I or those described in the measurements of dark metabolic flux of cGMP.

constructed from the convolution of two delay stages each of 0.045 s time constant and one delay stage of 0.2 s time constant. Three additional experiments gave very similar results; i.e., good agreement between the recorded and the predicted physiological dim flash responses. Thus, it appears that our simple model of the Ca^{2+} feedback can predict the size and shape of the physiological dim flash response reasonably well. Table II shows the parameters describing $\beta^*(t)$ in all five experiments. The variations in fitted time constants among different cells should not be taken too literally because they are quite sensitive to the shape of the derived $\beta^*(t)$, which is only approximate. The average peak value for $\beta^*(t)$ is 0.09 s^{-1} Rh^{*-1}. The last column in Table II, $\int \beta^*(t)\, dt$, with an average of 0.033 Rh^{*-1}, is useful later for calculating responses to steady light.

Adaptation to Background Light

From the results described so far, it is clear that the Ca^{2+} feedback functions in primate rods in much the same way as in amphibian rods, except for a difference in kinetics. In this section it is shown that primate rods also adapt to background light.

Fig. 7 *A* shows the responses of a typical rod from *M. fascicularis* to light steps of different intensities. In this kind of experiment, the recordings were all made by sucking a rod outer segment projecting from a fragment of retina into the recording pipette. The low-frequency noise in the traces was due to photon fluctuations. One prominent feature shown by the responses is the rapid relaxation from a transient peak, which is a sign of light adaptation. Both the magnitude and the time course (1–2 s) of relaxation are similar to those observed in rods of lower mammalian species

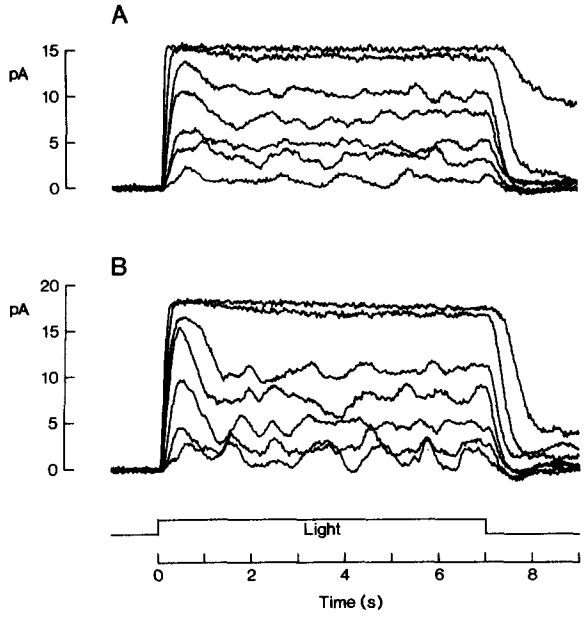

FIGURE 7. Step response families obtained from two *M. fascicularis* rods. In each case, the recordings were made from a rod outer segment projecting from a fragment of retina. (*A*) A fairly typical cell. Step intensities were 18, 64, 110, 240, 400, 850, and 3,400 Rh* s^{-1}, respectively. The corresponding responses were averages of 2, 2, 2, 2, 2, 1, and 1 trials. 38.5°C. (*B*) Cell with the most severe response relaxation. Step intensities were 18, 30, 110, 240, 400, 850, and 1600 Rh* s^{-1}, respectively. The corresponding responses were averages of 2, 2, 3, 2, 2, 1, and 1 trials. 38°C. DC-25 Hz in both cases.

(Nakatani et al., 1991). Apart from the faster kinetics, the general characteristics of these responses are also similar to those recorded from amphibian rods (see, for example, Baylor et al., 1980; Nakatani and Yau, 1988*b*). Fig. 7 *B* shows the results from another rod; this cell had the most severe response relaxations out of a total of 15 experiments.

Similar observations were made from rods of the other primate species, including the nocturnal *Galago*. Fig. 8 shows collected results from all four species in the form of normalized response–intensity relations at steady state. The smooth curve in each panel is drawn according to the exponential relation:

$$\hat{r}_S = 1 - e^{-k_S J_S} \tag{16}$$

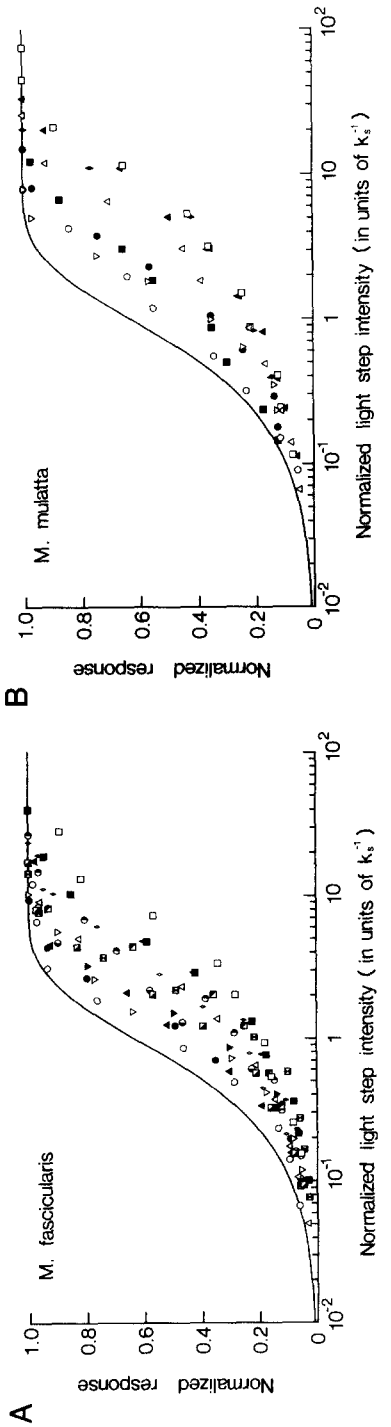

FIGURE 8. Collected step response–intensity relations at steady state, plotted on normalized axes, from 15 *M. fascicularis* rods (*A*), 8 *M. mulatta* rods (*B*), 5 *C. aethiops* rods (*C*), and 5 *G. garnetti* rods (*D*). Continuous curves in *A–D* are drawn from Eq. 16. Saturated photocurrent and temperature ranges are: 13–27 pA, 37–41°C (*A*); 11–25 pA, 38–41°C (*B*); 10–17.6 pA, 36.5–39°C (*C*); 7.6–12.1 pA, 37–39.5°C (*D*).

where $\hat{r}_S$ is the normalized step response, I_S is the step intensity, and k_S is a proportionality constant. This equation is derived from a statistical superposition of invariant responses to individual photons, and gives the expected response–intensity relation if there were no light adaptation (Lamb et al., 1981; Baylor et al., 1984; Tamura et al., 1989; Nakatani et al., 1991). The experimental relations clearly deviate from the smooth curve in that they are much gentler in form. There is a fair amount of variation in the degree of steepness of the relation among different cells. It is not clear whether this represents a genuine physiological variation among cells or whether the steeper relations (i.e., less adaptation) came from less healthy cells. For each cell in Fig. 8, the relative position between the curve and the experimental points is constrained by the relation $k_S = k_F \cdot t_i$, where t_i is the integration time of the dim flash response measured from that cell and k_F is its absolute sensitivity expressed as a fraction of the maximum response produced by one Rh* (see Baylor et al., 1984; Nakatani and Yau, 1988*b*; Tamura et al., 1989; Nakatani et al., 1991). On the average, the steady-state step response reached half-maximum at ~100–400 Rh* s^{-1}, and saturated at ~2,000–4,000 Rh* s^{-1} (see Table III). These values are not very different from those found for rods of lower mammalian species (Nakatani et al., 1991).

Another way to study background light adaptation consists of examining the change in flash sensitivity produced by background light. Fig. 9 shows the collected results from this type of experiment, again for all four primate species. Here flash sensitivity is plotted against background intensity in normalized log-log coordinates. The reduction in sensitivity is expressed as S_F/S_F^D, where S_F is the flash sensitivity in the presence of background light and S_F^D is the absolute flash sensitivity without background light (both in units of pA photon^{-1} μm^2). For each cell, S_F^D and S_F were determined from the cell's average response to typically 15–30 flash trials in darkness and in different backgrounds, with the test flash intensities adjusted to elicit just-detectable responses. The solid curve in each panel is drawn according to (see Baylor et al., 1980; Tamura et al., 1989; Nakatani et al., 1991):

$$S_F/S_F^D = \frac{1}{1 + I_S/I_O} \tag{17}$$

where I_S is the steady background intensity and I_O is a constant. This is the familiar Weber-Fechner relation describing background light adaptation. The dashed curve in each panel is drawn according to:

$$S_F/S_F^D = e^{-k_S I_S} \tag{18}$$

obtained by differentiating Eq. 16 with respect to I_S (and assuming constant integration time of the incremental flash response), and representing the relation expected from no background light adaptation (see Baylor et al., 1984; Tamura et al., 1989; Nakatani et al., 1991). It can be seen that the experimental data generally fit the Weber relation much better than the exponential relation. The average I_O values for the four species are all in the range of 30–50 Rh* s^{-1} (see Table III), close to that found in lower mammalian species (Nakatani et al., 1991). Overall, the inverse relation between incremental flash sensitivity and background light described by Eq. 17 was valid with sensitivity down to 1/25–1/100 of that in darkness, again not too

TABLE III

Collected Parameters for Light Responses of Rods of Different Primate Species

Rods	$j_{D,0}$	Single-photon response			Steady-state step response		Incremental flash on background
		Peak size	t_p	t_i	Half-saturating I_S	Saturating I_S	I_O
	pA	*pA*	*ms*	*ms*	*Rh* s*$^{-1}$	*Rh* s*$^{-1}$	*Rh* s*$^{-1}$
M. fascicularis	18.1 ± 3.8 (15)*	0.62 ± 0.21 (15)‡	234 ± 40 (15)	348 ± 91 (15)	280 ± 139 (15)	ca. 3,000 (15)§	52 ± 34 (10)
M. mulatta	18.1 ± 5.2 (8)*	0.97 ± 0.48 (8)‡	233 ± 47 (8)	313 ± 64 (8)	317 ± 102 (8)	ca. 3,000 (8)§	37 ± 24 (6)
C. aethiops	13.2 ± 3.1 (5)	0.77 ± 0.31 (5)‡	211 ± 44 (5)	334 ± 149 (5)	390 ± 162 (5)	ca. 4,000 (5)§	38 ± 17 (3)
G. garnetti	9.5 ± 1.7 (5)	0.59 ± 0.28 (5)‡	203 ± 18 (5)	298 ± 32 (5)	118 ± 83 (5)	ca. 2,000 (5)§	28 ± 10 (4)

Each entry shows the mean and the standard deviation; the number in parentheses indicates the number of cells studied. $j_{D,0}$, steady-state dark current; t_p, time to peak; t_i, integration time; I_S, steady light intensity; I_O, constant in the Weber-Fechner relation (Eq 17); Rh*, rhodopsin photoisomerizations. The numbers in Rh* were calculated from calibrated light intensities and an effective collecting area (transverse light incidence, unpolarized) of 0.8 μm^2 for rods of first three species and 0.35 μm^2 for *G. garnetti* rods.

*After being corrected for the imperfect current collection by the suction pipette (by dividing by 0.8; see Methods), these dark currents become ~22.5 pA. For simplicity, we adopted $j_{D,0}$ = 21 pA in the modeling, consisting of 20 pA of $j_{ch,0}$ and 1 pA of $j_{ex,0}$ (see Appendix).

‡These single-photon response amplitudes were estimated from the ratio σ^2/m, where σ^2 and m are the variance and the mean of the peak amplitudes of the responses to a series of identical dim flashes.

§These numbers are only rough values because of the asymptotic approach of the light response amplitude to saturation.

different from that found in the other mammals we have studied (Nakatani et al., 1991). The flash response showed slightly faster kinetics in the presence of background light, though any quantitation of the time course was difficult because of significant fluctuations in baseline due to the background photon noise.

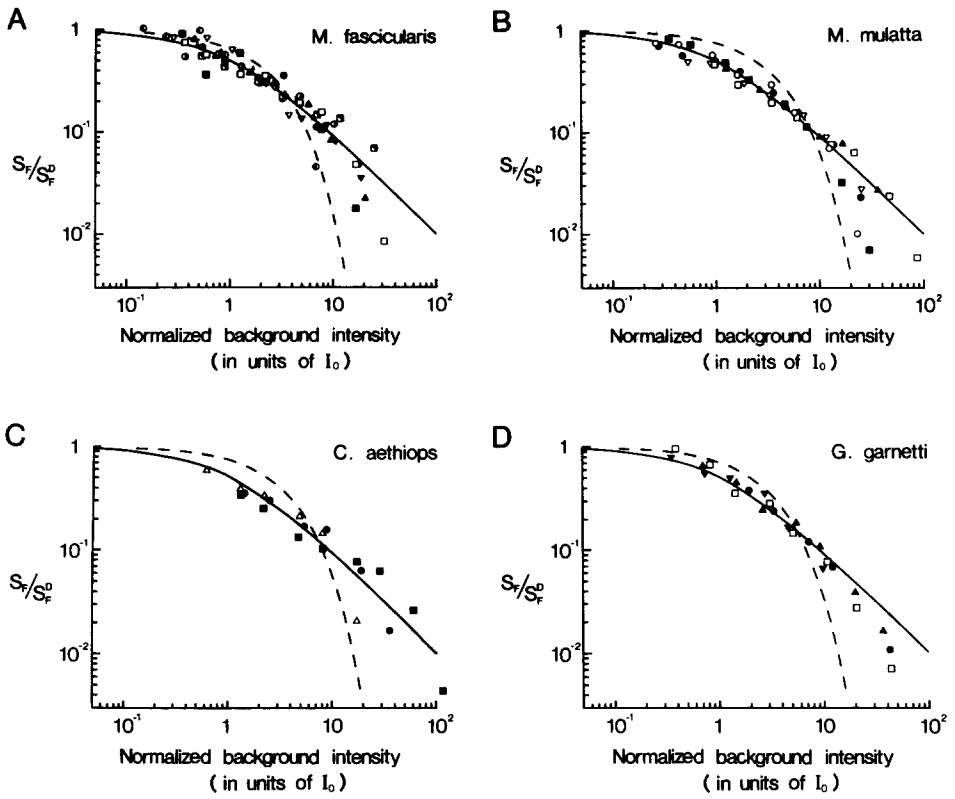

FIGURE 9. Collected results of incremental flash-on-background experiments, plotted on normalized axes, from 10 *M. fascicularis* rods (*A*), 6 *M. mulatta* rods (*B*), 3 *C. aethiops* rods (*C*), and 4 *G. garnetti* rods (*D*). Recordings made from outer segments projecting from retinal fragments. In each panel, solid curve is drawn from Eq. 17, and dashed curve is from Eq. 18. The position of the dashed curve relative to the experimental points represents the average position for all cells. Saturated photocurrent and temperature ranges are: 11.0–20.5 pA, 37–41°C (*A*); 10.7–25 pA, 38.5–41°C (*B*); 11.4–16.6 pA, 36.5–39°C (*C*); 6.0–12.2 pA, 37–39.5°C (*D*).

Prediction of Background Adaptation from the Ca^{2+} Feedback Model

For amphibian rods, we and others have previously shown that when the Ca^{2+} feedback is removed by using a 0 Na^+–0 Ca^{2+} external solution (see above), the phenomenon of background light adaptation essentially disappears (Matthews et al., 1988; Nakatani and Yau, 1988*b*; Fain et al., 1989). It would be nice if the same could be demonstrated for the primate rods studied here. However, this experiment so far has not been possible because of the extreme difficulty in recording from an isolated

primate rod for an extended period of time, a requirement for this kind of experiment. As an alternative, we took the more indirect approach of asking whether the background adaptation described in the previous section can be accounted for by the known characteristics of the Ca^{2+} feedback.

Assuming that $\beta^*(t)$, the time course of phosphodiesterase activity triggered by a photoisomerization, does not change with increasing light intensity (see Discussion), the response of a rod to a step of light can be obtained by convolving $\beta^*(t)$ with a step function of appropriate magnitude I_S (in units of Rh* s^{-1}) before the equations describing the Ca^{2+} feedback are applied. For calculations, we have chosen $\beta^*(t)$ with a peak value of 0.09 s^{-1} Rh^{*-1} and a waveform composed of three equal delay stages of 0.1 s time constant, essentially the average values in Table II. Fig. 10 shows the results of these computations, involving either two fast (*A*) or two slow (*B*) buffers; *C* will be described later. Oscillations are again present in the step response when rapid

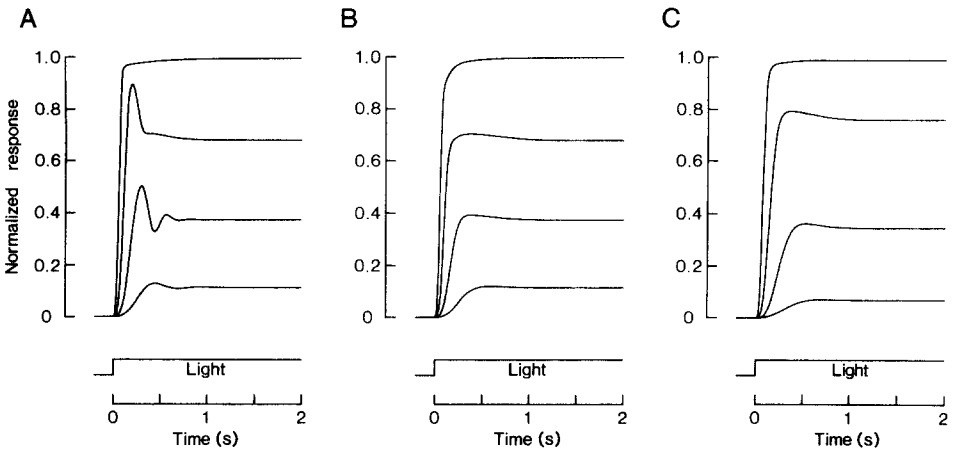

FIGURE 10. Computed step response families. Model consists of: (*A*) two fast Ca^{2+} buffers; (*B*) two slow Ca^{2+} buffers; (*C*) two slow Ca^{2+} buffers, but with Eq. 19 replacing Eq. A6 for describing the Ca^{2+} extrusion. Step intensities used for calculations are 30, 300, 3,000, and 30,000 Rh* s^{-1} in *A* and *B*, and 10, 100, 1,000, and 10,000 Rh* s^{-1} in *C*. See text for details.

buffers are considered. On the other hand, the relaxations shown by the responses in Fig. 10 *B* are broadly similar in time course to experimental observations (cf. Fig. 7 *A*), taking ~ 1 s to complete, though the transient peak is less than typically seen in experiments (cf. Fig. 7 *A*). Since the transient peak represents the cross-over between a fast-rising photocurrent and a relaxation due to adaptation, minor adjustments of the kinetic parameters for one or the other process should be all that is necessary to bring about a larger transient peak. We have not made an attempt to do this, however, because our primary objective here is to adhere to a simple scheme as well as experimentally derived parameters.

The plateau levels of the step responses in Fig. 10, *A* and *B*, are identical, as expected from the fact that in steady state the situations of fast and slow buffers become one and the same. Curve *1* in Fig. 11 *A* shows the complete step response–intensity relation in steady state derived from the computations described above. It is

similar to the experimentally measured relation (cf. Fig. 8) in that it is much gentler than the dashed curve, which is our standard curve for the situation of no background light adaptation (Eq. 16). The half-saturating step intensity obtained from the computed relation, at ~800 Rh* s^{-1}, is somewhat higher than the measured values (cf. Table III). An unusual feature of curve *1* is its sudden increase in steepness near the top. This feature can be understood from Eq. A9, which describes the relation between guanylate cyclase activity, α, and Ca_f. The gain of the Ca^{2+} feedback depends on the slope of this relation, that is, $-d\alpha/dCa_f$. It can be shown from Eq. A9 that $-d\alpha/dCa_f$ initially increases when Ca_f decreases from a high value, but reaches maximum at a certain value $\overline{Ca}_f$, given by $\overline{Ca}_f = K_{cy}[(m-1)/(m+1)]^{1/m}$. With $m = 4$, we obtain $\overline{Ca}_f = 0.88\ K_{cy}$, or equal to 88 nM with $K_{cy} = 100$ nM. When Ca_f decreases

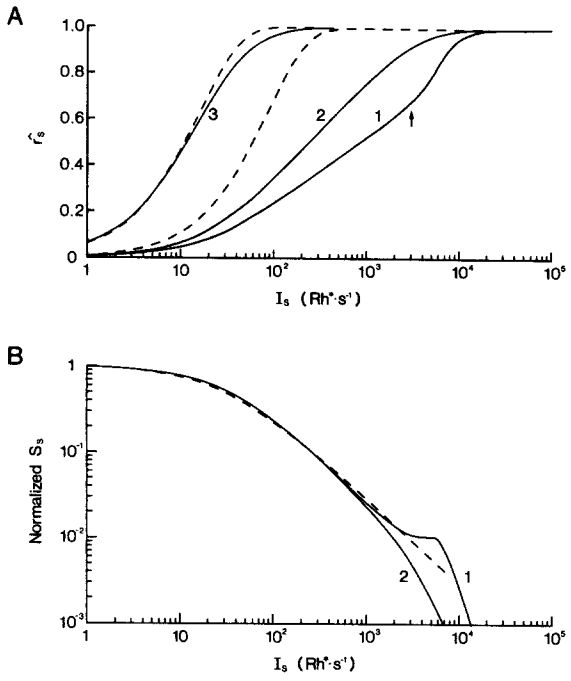

FIGURE 11. (*A*) Computed step response–intensity relations in steady state. Curve *1* corresponds to the situation in Fig. 10, *A* and *B*. Curve *2* corresponds to the situation in Fig. 10 *C*. Curve *3* is calculated from Eq. 22, derived by assuming no Ca^{2+} feedback. Both dashed curves are drawn from Eq. 16, but shifted to different positions on the abscissa to coincide with curves *1* (and *2*) and *3* at low intensities. Arrow is at 3,000 Rh* s^{-1}. See text for details. (*B*) Expected reduction in step sensitivity (S_S) by steady light, calculated as $\Delta\hat{r}_S/\Delta I_S$, from curves *1* and *2* in *A*. $\Delta\hat{r}_S/\Delta I_S$ has been normalized by its value at ~0.1 Rh* s^{-1}. Dashed curve is drawn according to Eq. 17 and displaced on the abscissa to provide the best fit to the two curves.

below $\overline{Ca}_f$, the slope and hence the feedback gain begin to decrease, producing a change in the trend of the step response–intensity relation at high intensities as indicated in Fig. 11 *A*. The value of Ca_f at different step light intensities can be directly obtained from the computations described above, and is found to reach 88 nM at $I_S \sim 3{,}000$ Rh* s^{-1}, indeed near the intensity at which curve *1* in Fig. 11 *A* begins to swing up (arrow). A few experiments in the collected step response–intensity relations of Fig. 8 perhaps showed signs of such a change in steepness near the top of the relation, but the majority of experiments did not.

A simple way to remove the upswing is to impose the restriction that Ca_f cannot decrease below a certain value C_0. Even though Cervetto et al. (1989) have argued that in equilibrium the Na^+–Ca^{2+} exchange can reduce Ca_f down to as low as 0.2 nM

in bright light because of the actual exchange stoichiometry being $4Na^+ : 1Ca^{2+}, 1K^+$ (see also Appendix), the value so far measured experimentally is considerably higher (~140 nM; see Ratto et al., 1988). This discrepancy may be due to a number of factors. One is the very low binding rate between Ca^{2+} and the exchange molecule at low Ca_f, so that equilibrium is only reached after a long time, well beyond the time frame of the typical experiment. Another is a steady internal release of Ca^{2+} from some unknown pool when Ca_f drops below a critical level. Finally, there may be a steady leakage of Ca^{2+} from the inner segment into the outer segment. To prevent Ca_f from dropping below C_0, Eq. A6 might formally be replaced with:

$$j_{ex} = J_{ex}\left[\frac{Ca_f - C_0}{(Ca_f - C_0) + K_{ex}}\right] \tag{19}$$

For convenience, we adopt $C_0 = K_{cy} = 0.1$ μM. This equation has the attraction that it retains the overall Michaelis relation, so that modifications in the computations described earlier are straightforward. The form of Eq. 19 may also be interpreted in the following way. Suppose for simplicity that there is a constant Ca^{2+} leakage, L, from the inner segment into the outer segment; then in bright light Ca_f will not decrease below C_0 when the efflux through the exchange (according to Eq. A6) is balanced by this inward leak. That is,

$$\frac{C_0}{C_0 + K_{ex}} = L$$

Thus, at $Ca_f > C_0$, the net efflux F_x is given by:

$$F_x \propto \frac{Ca_f}{Ca_f + K_{ex}} - L$$

$$\propto \frac{Ca_f}{Ca_f + K_{ex}} - \frac{C_0}{C_0 + K_{ex}}$$

$$\propto \frac{Ca_f - C_0}{(Ca_f - C_0) + (K_{ex} + C_0)} \simeq \frac{Ca_f - C_0}{(Ca_f - C_0) + K_{ex}}, \qquad \text{for } C_0 \ll K_{ex}$$

F_x and j_{ex} are identical if the inward leak is formally incorporated as a characteristic of the exchange current. Eq. 19 can be used in place of Eq. A6 to fit the results of the Ca^{2+} efflux experiments shown in Figs. 2 and 3, and can produce a practically identical time course of decline for the exchange current as with Eq. A6, except different values for the R_T's and K_D's have to be adopted. Table I, part *C* collects the appropriate numbers for curve-fitting all experiments of this kind using Eq. 19; the averages from these are used to generate trace *d* (dotted) in Fig. 6, *C* and *F*, as well as the step responses in Fig. 10 *C*. These computed responses are very similar to those produced from earlier calculations. Finally, Eq. 19 produces curve *2* in Fig. 11 *A*, which lacks the upswing at high intensities. The half-saturating step intensity measured from curve *2* is ~250 Rh* s^{-1}, which is fairly close to the measured values (see Table III).

Curve *3* in Fig. 11 *A* shows the response–intensity relation computed without imposing the Ca^{2+} feedback at all. In this case, using Eq. A14 and setting $dG/dt = 0$

(for steady state) and $Ca_f = Ca_{f,0}$ (for the absence of Ca^{2+} feedback), we get, after rearranging terms:

$$G = \frac{\beta_0 G_0}{\beta_0 + I_S \int \beta^*(t)\, dt} \tag{20}$$

The normalized step response, $\hat{r}_S$, is given by:

$$\hat{r}_S = 1 - j_D/j_{D,0} \tag{21}$$

Since $j_{ex} = 0$ under these conditions, and $j_{ch} = (J_{ch}/K_{ch}^n)G^n$, we have (see also Forti et al., 1989):

$$\begin{aligned} \hat{r}_S &= 1 - j_{ch}/j_{ch,0} \\ &= 1 - (G/G_0)^n \\ &= 1 - \left(\frac{\beta_0}{\beta_0 + I_S \int \beta^*(t)\, dt}\right)^n \end{aligned} \tag{22}$$

Curve *3* in Fig. 11 *A* is drawn from Eq. 22 using $n = 2.5$, $\beta_0 = 1.2\ s^{-1}$, and $\int \beta^*(t)dt = 0.033\ Rh^{*-1}$. It is surprisingly similar to the dashed curve; that is, Eq. 16, even though the present calculations assume spatial homogeneity in the rod outer segment (see Appendix), whereas Eq. 16 was originally derived based on strict spatial compartmentalization of the phototransduction process (Lamb et al., 1981). As pointed out earlier, we have no experimental data from primate rods on the step response–intensity relation in the absence of Ca^+ feedback, but the roughly 20-fold difference in half-saturating step intensity between the computed curves *2* and *3* is not very different from that previously measured in experiments on toad rods (see Nakatani and Yau, 1988*b*).

The slope of the step response–intensity relation, $d\hat{r}_S/dI_S$, gives the step sensitivity, S_S. The flash sensitivity, S_F, is given by $S_S = S_F \cdot t_i$, where t_i is the integration time (Baylor and Hodgkin, 1973). Since, however, t_i changes only slightly (see above) compared with the large change in S_S, we can write, approximately, $S_F \propto S_S$. Curve *1* in Fig. 11 *B* shows the normalized S_S ($\sim S_F$) calculated from curve *1* in Fig. 11 *A* and plotted against the step intensity I_S; the normalization of S_S has been made against the value of S_S at an arbitrarily low I_S (0.1 $Rh^*\ s^{-1}$) where sensitivity is essentially the same as in darkness. This relation shows a curious region of constant sensitivity between ~3,000 and 6,000 $Rh^*\ s^{-1}$, which in fact corresponds to the upswing of curve *1* in Fig. 11 *A*. Curve *2* in Fig. 11 *B*, which is derived from curve *2* in Fig. 11 *A*, does not have this oddity. The dashed curve in Fig. 11 *C* shows the Weber-Fechner relation, i.e., Eq. 17. It agrees with the computed curves *1* and *2* quite well, roughly over 100-fold reduction in sensitivity from darkness. The I_O value obtained from either curve *1* or *2* is ~35 $Rh^*\ s^{-1}$, again similar to experimentally measured values (cf. Table III).

A more elaborate way to evaluate S_F in different background lights, without involving the integration time, is to repeat the computations for flash responses as previously described, but with β_0 in Eq. A14 replaced by $\beta_0 + I_S \int \beta^*(t)dt$, which

represents the total steady-state metabolic flux rate for cGMP at a certain background I_S. The resulting relation (not shown) is very similar to curves *1* and *2* in Fig. 11 *B*.

In summary, our model of the Ca^{2+} feedback appears to be able to account reasonably well for the behavior of primate rods to background light.

DISCUSSION

Ca^{2+} Feedback and Phototransduction

There is no doubt that a negative feedback mediated by Ca^{2+} fluxes regulates light sensitivity in primate rods as it does in amphibian rods. On the simple idea that this feedback works entirely via a negative modulation of the guanylate cyclase enzyme by Ca^{2+}, we were able to account for the size and shape of the cells' physiological responses to a dim flash as well as the relation between sensitivity reduction and background light intensity reasonably well. This agreement between theory and observation, though indirect, suggests that in primate rods, as in amphibian rods (Matthews et al., 1988; Nakatani and Yau, 1988*b*), the Ca^{2+} feedback is probably the primary mechanism regulating rod sensitivity at nonbleaching light levels.

Recently, Forti et al. (1989) and Sneyd and Tranchina (1989) have carried out detailed theoretical studies of the light response of amphibian rods and cones. Compared with the work of Forti et al. (1989), our modeling is perhaps a bit simplistic in that we have not examined some of the complexities present in the decline phase of responses to saturating light. However, we are primarily interested in whether the various parameters for the phototransduction mechanism that we have experimentally derived can be put together to make reasonable predictions about the overall behavior of the rods. We have therefore adhered to a simple scheme and deliberately avoided free choices of parameters as much as possible. For example, the parameters we have chosen for describing Ca^{2+} buffering are obtained by curve-fitting the observed time course of decline of the exchange current. At the same time, we extracted the time course of the light-activated phosphodiesterase activity ($\beta^*(t)$ in Results) directly from the dim flash response measured in the absence of the Ca^{2+} feedback. While not explicitly shown in their paper, the theoretical time course for $\beta^*(t)$ adopted by Forti et al. (1989) can be derived from their equations and shows a fast rising phase followed by a very slow, prolonged decline phase. This time course is much more asymmetrical about the peak compared with what we derived (see Fig. 6, *B* and *E;* also Fig. 7 in Hodgkin and Nunn, 1988). Our $\beta^*(t)$ is probably more accurate, though its more symmetrical form tends to produce oscillations in the light response, such as indicated by trace *b* in Fig. 6, *C* and *F*. However, these oscillations can be significantly reduced or eliminated by slowing down the kinetics of intracellular Ca^{2+} buffering, as described in the Results; it would, nonetheless, be extremely difficult to confirm the true values of these kinetic rates from direct measurements. It may also be pointed out that while oscillations are rarely seen in amphibian rod responses, we have actually observed them quite frequently when initially recording from a primate rod (13 of 22 cells from *M. fascicularis,* 3 of 9 cells from *M. mulatta,* 1 of 6 cells from *C. aethiops,* and 2 of 7 cells from *G. garnetti*). An example of these oscillations is shown in Fig. 12, recorded from a *M. fascicularis* rod. These oscillations are reminiscent of those observed in primate

cone responses (Schnapf et al., 1990), but in rods they tend to disappear over a period of minutes during recording. One possible reason for their disappearance is that the kinetics of Ca^{2+} buffering, or possibly extrusion, slowed down with time during experiments; some evidence for a possible slowing down of Ca^{2+} extrusion with time during recording has been reported by Hodgkin et al. (1987). It is difficult to decide at present whether the oscillations in primate rod responses are physiological or not.

Several assumptions in our theoretical analysis deserve further comment. First, we have assumed the phosphodiesterase activity induced by a photon to be constant all the way up to saturation of the light response. This assumption is based on in vitro biochemical measurements (Barkdoll et al., 1989) showing that the phosphodiesterase activation is linear with light intensities at least up to a 10^{-4} bleach of pigment content, corresponding to well over 10^4 Rh*. For an integration time of ~ 0.3 s ($\int \beta^*(t)dt/\beta^*_{peak}$) in primate rods, the phosphodiesterase activation by steady light should therefore be linear at least up to 3×10^4 Rh* s^{-1}, an intensity that already saturates the light response. In the intact cell, of course, some unknown modulation

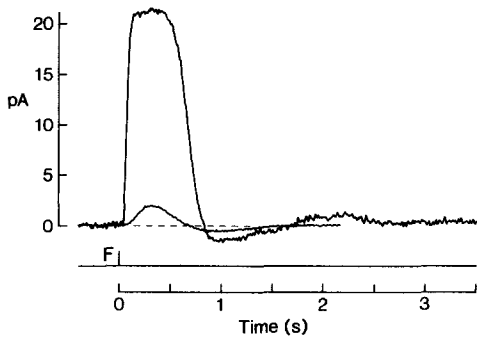

FIGURE 12. Flash responses from a *M. fascicularis* rod to illustrate the oscillations frequently observed in the decline phase of the responses. Recordings were made from an outer segment projecting from a retinal fragment. Flash (*F*) delivered at time zero, producing 2.6 Rh* in the dim case and 280 Rh* in the bright case; corresponding responses represent averages of 30 and 2 flash trials, respectively. 38°C. DC-40 Hz.

of the enzyme by background light may still exist. For instance, Nicol and Bownds (1989) found that the light response kinetics of rods speeded up with background light in conditions where internal Ca^{2+} was not supposed to change. One possible reason for this would be a change in the activation/deactivation kinetics of the phosphodiesterase. Second, the adoption of Eq. A10 for describing the cyclase modulation by Ca^{2+} is just an approximation. It has the attraction of being simple, and is broadly consistent with the in vitro observations of Koch and Stryer (1988). However, uncertainty remains about the quantitative relation describing the modulation under physiological conditions, in particular for internal Ca^{2+} concentrations near the dark value and higher. This point is discussed further in the Appendix. Third, there may well be other ways to remove the anomalous change in steepness of curve *1* in Fig. 11 *A* besides imposing a lower limit (C_0) for the decrease of intracellular Ca^{2+}. However, such measures would probably involve other assumptions or modifications of parameters, which we try to avoid. Furthermore, as pointed out in the Results, there is some experimental evidence (Ratto et al., 1988) that internal Ca^{2+} may not decrease below ~ 0.1 μM with steady light, at least within the experimental time scale.

A more serious concern has to do with the assumption of spatial homogeneity in the outer segment. There is evidence that the effect of a photon is spatially restricted in the outer segment (Lamb et al., 1981; Matthews, 1986). On the other hand, no quantitative information on the diffusion of Ca^{2+} and cGMP in the outer segment is yet available for incorporation into the theory. In steady bright light, however, when the outer segment should experience fairly uniform excitation along its length, this may be less of a concern (see also Forti et al., 1989). In any case, it is interesting that theory and observation agree quite well despite the simplifying assumption. Furthermore, in the absence of Ca^{2+} feedback, the step response–intensity relation in steady state derived from spatial homogeneity (Eq. 22 in the Results; see also Forti et al., 1989) is remarkably similar in form to that derived from the assumption of a strict spatial compartmentalization of photoexcitation (Eq. 16). These agreements may make it difficult in the future to evaluate the contribution of restricted diffusion to light response properties.

Finally, we have ignored the bound pool of cGMP within the outer segment in the modeling. Again, the reason is that too little is known at present, apart from the belief that as much as 90% of the total cGMP in the outer segment is bound (Yau and Nakatani, 1985*b;* Nakatani and Yau, 1988*c*), probably to the high-affinity, noncatalytic sites on the cGMP phosphodiesterase (Yamazaki et al., 1980). If the bound pool(s) stays constant regardless of changes in the free pool, however, then ignoring the former should not make any difference. Even though this assumption is probably not strictly correct (see Cote et al., 1986), the supporting evidence is that only very small changes in total cGMP are detected in rods even when the light is bright enough to close all the cGMP-gated channels (see, for example, Kilbride and Ebrey, 1979; Goldberg et al., 1983; Blazynski and Cohen, 1986). The dark cGMP phosphodiesterase activity derived from our experiments is $\sim 1.2\ s^{-1}$. With the free cGMP concentration at several micromoles per liter (Yau and Nakatani, 1985*b;* Nakatani and Yau, 1988*c*), the rate of basal cGMP hydrolysis in darkness should therefore be $\sim 10\ \mu M\ s^{-1}$, which agrees fairly well with that measured in the intact rabbit retina using the ^{18}O incorporation technique ($\sim 14\ \mu M\ s^{-1}$; see Ames et al., 1986). Furthermore, the time-integrated phosphodiesterase activity, $\int \beta^*(t)dt$, stimulated by light is $\sim 0.033\ Rh^{*-1}$ from our experiments, which translates into $\sim 0.3\ \mu M$ cGMP Rh^{*-1}, or $\sim 5{,}000$ cGMP molecules hydrolyzed during the response time course to one photoisomerization (calculated from a free cytosolic volume of $\sim 30\ \mu m^3$). This again compares favorably with the value of $\sim 10^4$ measured biochemically in the intact retina (Ames et al., 1986). If the 10-fold excess of bound cGMP were to exchange rapidly with free cGMP, our estimates (derived by ignoring bound cGMP) would have been only $\sim 10\%$ of the biochemical estimates.

Background Adaptation in Mammalian Rods

There has been a long history of confusion about whether mammalian rods adapt to light as do rods of cold-blooded vertebrates (briefly reviewed in Tamura et al., 1989; Nakatani et al., 1991). Based on our studies of many mammalian species, including the primates reported here, there is no doubt that these cells do adopt (see also Tamura et al., 1989; Nakatani et al., 1991), though the range of background light

intensities over which the Weber law applies may be slightly narrower for mammalian rods than for, say, amphibian rods. We have also pointed out in earlier papers (Tamura et al., 1989; Nakatani et al., 1991) that in cone-sparse retinas, such as those of rat, cat, and rabbit, there is a need for rods to adapt at mesopic light levels in order to avoid any discontinuity in visual function resulting from the high threshold of the cone system. As for humans, the macaque and other primates with relatively cone-rich retinas, the adaptational property of rods is probably not as important, at least for normal foveal and parafoveal vision, because the abundance of cones in these retinal regions produces a relatively low threshold for the cone system (Stiles, 1959). Exception, however, may be taken for unusual lighting conditions that selectively desensitize the cones (Aguilar and Stiles, 1954) and for vision in the periphery of the retina.

Finally, it is interesting that rods of the nocturnal *Galago* behave in much the same way as rods of the other three primate species studied here, which are all diurnal. Furthermore, the rod adaptation observed in all four species is quantitatively similar to that previously found in lower mammals (see Nakatani et al., 1991). This stereotypic behavior suggests that the degree of adaptation in individual rods is perhaps already optimized across species, allowing sufficiently high sensitivity for night vision and at the same time providing Weber behavior (to achieve constancy in contrast sensitivity; see Shapley and Enroth-Cugell, 1984) over about 2 log units of background intensity for flexibility (see Results here and Tamura et al., 1989; Nakatani et al., 1991). Combined with adaptation at the network level, the overall Weber range for the rod system spans a reasonably broad 5 log units of background intensity (see, for example, Aguilar and Stiles, 1954; Fuortes et al., 1961; Enroth-Cugell et al., 1977). There is a trade-off between sensitivity and dynamic range. A weaker Ca^{2+} feedback would increase sensitivity in darkness and dim background light, but reduce the dynamic range because response saturation would be rapidly reached. A stronger feedback, on the other hand, could extend the dynamic range, but at the expense of sensitivity at low light levels. The rods appear to have evolved into a compromise between the two requirements. To further extend the dynamic range of vision into brighter light intensities as required by the behaviors of different animal species, a cone system of varied importance is introduced instead of modifying the properties of the rod system. In this regard, it is interesting to note that even the nocturnal *Galago,* traditionally thought to lack cones, has in fact been found recently to have these receptors in its retina, though to a lesser degree than its diurnal counterparts (Wikler and Rakic, 1990).

APPENDIX

We introduce here the basic equations used in the Results for describing the feedback action generated by Ca^{2+} fluxes on the rod light response. The key features of this Ca^{2+} feedback are summarized in Fig. 13, which shows a Ca^{2+} influx through the cGMP-activated conductance and an efflux through the Na^+–Ca^{2+} exchange. The cytosolic free Ca^{2+}, which exerts a negative modulation on the guanylate cyclase, is assumed to exchange with Ca^{2+} bound to a buffer (which does not necessarily represent the entire bound pool of internal Ca^{2+}). In what follows, spatial inhomogeneities in the outer segment are ignored for lack of complete information and

for simplifying the analysis. Also, we have not considered the bound pool of cGMP, about which little is known (but see Discussion). Finally, apart from the parameters described in the Results, the numerical values used in the analysis are mostly derived from experiments on amphibian rods. However, since the parameters borrowed from amphibian rods are all equilibrium parameters, whereas the only obvious difference in phototransduction between amphibian and mammalian rods resides in the kinetics, this treatment does not seem too far-fetched. Previously, the effect of the Ca^{2+} feedback on phototransduction has been examined in various degrees of detail in amphibian rods (Hodgkin, 1988; Hodgkin and Nunn, 1988; Forti et al., 1989) and amphibian and primate cones (Sneyd and Tranchina, 1989; Schnapf et al., 1990). Our approach here is in many ways similar to that of Forti et al. (1989).

Consider the following Ca^{2+} buffering reaction:

$$Ca + R \underset{k_{off}}{\overset{k_{on}}{\rightleftharpoons}} Ca\,R$$

We can write:

$$\begin{aligned} dCa_b/dt &= k_{on}Ca_fR_f - k_{off}Ca_b \\ &= k_{on}Ca_f(R_T - Ca_b) - k_{off}Ca_b \end{aligned} \tag{A1}$$

where Ca_f and Ca_b are the free and bound Ca^{2+} concentrations, R_f and R_T are the free and total buffer concentrations, and k_{on} and k_{off} are the binding and unbinding rates.

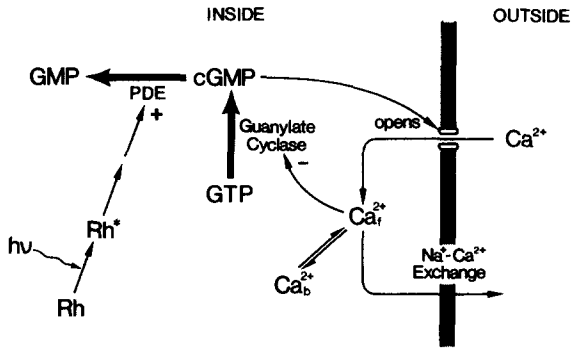

FIGURE 13. Scheme showing the Ca^{2+} feedback mechanism in rod phototransduction. *Rh*, rhodopsin; *Rh**, photoisomerized rhodopsin; *hν*, photon; *PDE*, phosphodiesterase; Ca_f^{2+}, free Ca^{2+}; Ca_b^{2+}, bound Ca^{2+}; +, activation; −, inhibition.

If the free and bound Ca^{2+} are in rapid equilibrium, $dCa_b/dt = 0$, and Eq. A1 reduces to:

$$Ca_b = \frac{Ca_fR_T}{Ca_f + K_D}$$

where $K_D \equiv k_{off}/k_{on}$ is the dissociation constant. The total Ca^{2+} concentration, Ca_T, is therefore given by:

$$Ca_T = Ca_f + Ca_b = Ca_f\left(1 + \frac{R_T}{Ca_f + K_D}\right) \tag{A2}$$

The change in Ca_T reflects the difference between Ca^{2+} influx and efflux, and can

be written as:

$$\begin{aligned} dCa_T/dt &= (1/FV)(j_{Ca}/2 - j_{ex}) \\ &= (1/FV)(0.1j_{ch}/2 - j_{ex}) \end{aligned} \tag{A3}$$

where j_{ex} is the exchange current, j_{Ca} is the Ca^{2+} component (taken to be 10%; see Results) of the current j_{ch} through the conductance (Yau and Nakatani, 1985*a*; Nakatani and Yau, 1988*a*), F is Faraday's constant, and V is the cytosolic volume of the outer segment. The dependence of j_{ch} on free cGMP concentration can be described approximately by the Hill equation (see Yau and Baylor, 1989, for review):

$$j_{ch} = J_{ch}\left(\frac{G^n}{G^n + K_{ch}^n}\right) \tag{A4}$$

where J_{ch} is the current through the maximally activated conductance, G is free cGMP concentration, K_{ch} is the half-saturating cGMP concentration, and n is the Hill coefficient. At G values near or greater than K_{ch}, the Hill equation deviates somewhat from the experimentally derived relation (see, for example, Nakatani and Yau, 1988*c*), but this is irrelevant here because under physiological conditions $G \ll K_{ch}$ (see Nakatani and Yau, 1988*c*), which also leads to the following approximation:

$$j_{ch} = \left(\frac{J_{ch}}{K_{ch}^n}\right) G^n \tag{A5}$$

As for the exchange current, j_{ex}, we adopt a Michaelis dependence on Ca_f (Lagnado et al., 1988):

$$j_{ex} = J_{ex}\left(\frac{Ca_f}{Ca_f + K_{ex}}\right) \tag{A6}$$

where J_{ex} is the saturated exchange current and K_{ex} is the Ca_f that would half-saturate the exchange. Eq. A6 predicts that in bright light Ca_f will eventually decrease to zero due to the exchange. In reality, however, this is not expected to happen because the exchange activity will stop when electrochemical equilibrium is reached. Based on their finding that the stoichiometry of the exchange is really $4Na^+$: $1Ca^{2+}$, $1K^+$, Cervetto et al. (1989) concluded that equilibrium will be reached at $Ca_f \simeq 0.2$ nM. The experimental value so far reported, however, is considerably higher (~ 140 nM; see Ratto et al., 1988). In the Results, a modification of Eq. A6 is also used to accommodate this feature.

Combining Eqs. A3, A5, and A6, we get:

$$\frac{dCa_T}{dt} = \left(\frac{1}{FV}\right)\left[0.05\left(\frac{J_{ch}}{K_{ch}^n}\right) G^n - J_{ex}\left(\frac{Ca_f}{Ca_f + K_{ex}}\right)\right] \tag{A7}$$

The rate of change in cGMP concentration, dG/dt, is given by the difference between synthesis and hydrolysis; that is:

$$dG/dt = \alpha - \beta G \tag{A8}$$

where α and β represent the rates of the two processes. The rate of synthesis depends on the concentration of GTP, the precursor of cGMP. This, however, is generally well buffered, so we assume it to be constant and absorb it into α. The guanylate cyclase also shows inhibition by Ca^{2+} acting cooperatively (Koch and Stryer, 1988; Kawamura and Murakami, 1989). An approximate expression for the observed inhibition is given by (see Forti et al., 1989 for a similar treatment):

$$\alpha = \frac{\alpha_{max}}{1 + (Ca_f/K_{cy})^m} \tag{A9}$$

where α_{max} is the maximally disinhibited rate of cGMP synthesis by guanylate cyclase, K_{cy} is the Ca_f that half-inhibits the guanylate cyclase, and m is the cooperativity, which is near 4 according to Koch and Stryer (1988). Expressing α as a function of its steady-state value in darkness, α_0, we can write:

$$\alpha = \alpha_0 \left[\frac{1 + (Ca_{f,0}/K_{cy})^m}{1 + (Ca_f/K_{cy})^m}\right] \tag{A10}$$

where $Ca_{f,0}$ is the free Ca^{2+} concentration in darkness. According to Eq. A10, $\alpha \rightarrow 0$ at high Ca_f. Biochemical measurements in vitro have indicated that some basal cyclase activity exists even at high Ca_f (see Koch and Stryer, 1988). Thus, a more realistic description of α may involve an additional term $f\alpha_{max}$ on the right side of Eq. A9, where $0 < f < 1$. The results of Koch and Stryer (1988) suggest that f should be ~ 0.2, but their experiments were carried out at a very high Mg^{2+} concentration (11 mM), which may not apply to the physiological situation. Furthermore, their results indicate that the cyclase activity does not decrease further when the Ca^{2+} concentration goes above 0.1 μM, whereas physiological experiments (see Fig. 5 and related text here; also Yau and Nakatani, 1984*a*; Hodgkin et al., 1985) suggest that the dark enzyme activity should decrease at least several-fold when Ca_f increases above the physiological value (~ 0.3 μM; see below). For simplicity, we retain Eq. A9 by setting f equal to 0.

The hydrolysis of cGMP represents the sum of dark- and light-stimulated phosphodiesterase activities; that is:

$$\beta = \beta_0 + \beta^*(t)I_F \tag{A11}$$

where β_0 is the dark hydrolytic rate and $\beta^*(t)$ is the additional rate triggered by one photon. The light-activated rate is assumed to increase proportionally with the photon content I_F of a flash. For the light intensities we are considering in this paper ($< 10^4$ photoisomerizations s^{-1}), this seems to be a reasonable assumption judging from biochemical measurements (Barkdoll et al., 1989; see also Discussion). Substituting Eqs. A10 and A11 in Eq. A8, we get:

$$\frac{dG}{dt} = \alpha_0 \left[\frac{1 + (Ca_{f,0}/K_{cy})^m}{1 + (Ca_f/K_{cy})^m}\right] - [\beta_0 + \beta^*(t)I_F]G \tag{A12}$$

Note that in steady state in darkness, $dG/dt = \beta^*(t) = 0$, and we can write:

$$\alpha_0 = \beta_0 G_0 \tag{A13}$$

where G_0 is the cGMP concentrations in darkness. Eq. A12 can therefore be rewritten as:

$$\frac{dG}{dt} = \beta_0 G_0 \left[\frac{1 + (Ca_{f,0}/K_{cy})^m}{1 + (Ca_f/K_{cy})^m}\right] - [\beta_0 + \beta^*(t)I_F]G \tag{A14}$$

Finally, the total dark membrane current at the outer segment, j_D, is given by the sum of the channel current and the exchange current; that is:

$$j_D = j_{ch} + j_{ex} \tag{A15}$$

Eqs. A7, A14, and A15, together with A1 or A2 or their variations, are used in the Results to compute the effect of the Ca^{2+} feedback. The numerical values for some of the parameters are derived in the Results. The others are adopted as follows. We take K_{ch} = 50 μM and n = 2.5, based on truncated-rod experiments with amphibian cells (Nakatani and Yau, 1988*c*) and excised-patch experiments with bovine rods (Lühring and Kaupp, 1989). Assuming that the physiological j_{ch} in darkness, $j_{ch,o}$, is nominally 20 pA (see Table III legend), and that this represents 1% of J_{ch} (Yau and Nakatani, 1985*b*; Nakatani and Yau, 1988*c*) we get $J_{ch} = 2 \times 10^3$ pA. From Eq. A5, then, we obtain G_0 = 7.9 μM. Also, from Eq. A3 and $j_{ch,0}$ = 20 pA, we get $j_{ex,0}$ = 1 pA, where $j_{ex,0}$ is the steady-state exchange current in darkness. Thus, $j_{D,0}$ = 21 pA. Finally, we adopt $Ca_{f,0}$ = 0.3 μM (McNaughton et al., 1986; Ratto et al., 1988; Korenbrot and Miller, 1989; Rispoli et al., 1990), and K_{cy} = 100 nM, m = 4 (Koch and Stryer, 1988).

We want to thank R. S. Dhallan for suggesting the method of inserting a glass fiber into the suction pipette, as shown in Fig. 1. We also thank Drs. K. Johnson, V. Mountcastle, and M. Steinmetz for providing us with some of the monkey eyes at the end of their experiments.

This work was supported by a grant from the U.S. National Eye Institute.

Original version received 26 September 1990 and accepted version received 22 January 1991.

REFERENCES

Aguilar, M., and W. S. Stiles. 1954. Saturation of the rod mechanism at high levels of stimulation. *Optica Acta.* 1:59–65.

Ames, A., III, T. F. Walseth, R. A. Heyman, M. Barad, R. M. Graeff, and N. D. Goldberg. 1986. Light-induced increases in cGMP metabolic flux correspond with electrical responses of photoreceptors. *Journal of Biological Chemistry.* 261:13034–13042.

Barkdoll, A. E., E. N. Pugh, and A. Sitaramayya. 1989. Calcium dependence of the activation and inactivation kinetics of the light-activated phosphodiesterase of retinal rods. *Journal of General Physiology.* 93:1091–1108.

Baylor, D. A., and A. L. Hodgkin. 1973. Detection and resolution of visual stimuli by turtle photoreceptors. *Journal of Physiology.* 234:163–198.

Baylor, D. A., T. D. Lamb, and K.-W. Yau. 1979*a*. The membrane current of single rod outer segments. *Journal of Physiology.* 288:589–611.

Baylor, D. A., T. D. Lamb, and K.-W. Yau. 1979*b*. Responses of retinal rods to single photons. *Journal of Physiology.* 288:613–634.

Baylor, D. A., G. Matthews, and K.-W. Yau. 1980. Two components of electrical dark noise in toad retinal rod outer segments. *Journal of Physiology.* 309:591–621.

Baylor, D. A., B. J. Nunn, and J. L. Schnapf. 1984. The photocurrent, noise and spectral sensitivity of rods of the monkey *Macaca fascicularis*. *Journal of Physiology*. 357:575–607.

Blazynski, C., and A. I. Cohen. 1986. Rapid declines in cyclic GMP of rod outer segments of intact frog photoreceptors after illumination. *Journal of Biological Chemistry*. 261:14142–14147.

Capovilla, M., L. Cervetto, and V. Torre. 1982. Antagonism between steady light and phosphodiesterase inhibitors on the kinetics of rod photoresponses. *Proceedings of the National Academy of Sciences, USA*. 79:6698–6702.

Cervetto, L., L. Lagnado, and P. A. McNaughton. 1987. Activation of the Na:Ca exchange in salamander rods by intracellular Ca. *Journal of Physiology*. 382:135P.

Cervetto, L., L. Lagnado, R. J. Perry, D. W. Robinson, and P. A. McNaughton. 1989. Extrusion of calcium from rod outer segments is driven by both sodium and potassium gradients. *Nature*. 337:740–743.

Cervetto, L., and P. A. McNaughton. 1986. The effect of phosphodiesterase inhibitors and lanthanum ions on the light-sensitive current of toad retinal rods. *Journal of Physiology*. 370:92–109.

Cote, R. H., G. D. Nicol, S. A. Burke, and M. D. Bownds. 1986. Changes in cGMP concentration correlates with some, but not all, aspects of the light-regulated conductance of frog rod photoreceptors. *Journal of Biological Chemistry*. 261:12965–12975.

Dartnall, H. J. A. 1972. Photosensitivity. *In* Photochemistry of Vision. H. J. A. Dartnall, editor. Springer Verlag, New York. 122–145.

Enroth-Cugell, C., B. G. Hertz, and P. Lennie. 1977. Cone signals in the cat's retina. *Journal of Physiology*. 269:273–296.

Fain, G. L., T. D. Lamb, H. R. Matthews, and R. L. W. Murphy. 1989. Cytoplasmic calcium as the messenager for light adaptation in salamander rods. *Journal of Physiology*. 416:215–243.

Forti, S., A. Menini, G. Rispoli, and V. Torre. 1989. Kinetics of phototransduction in retinal rods of the newt *Triturus cristatus*. *Journal of Physiology*. 419:265–295.

Fuortes, M. G. F., R. D. Gunkel, and W. A. H. Rushton. 1961. Increment thresholds in a subject deficient in cone vision. *Journal of Physiology*. 156:179–192.

Gold, G. H. 1986. Plasma membrane calcium fluxes in intact rods are inconsistent with the calcium hypothesis. *Proceedings of the National Academy of Sciences, USA*. 83:1150–1154.

Goldberg, N. D., A. Ames III, J. E. Gander, and T. F. Walseth. 1983. Magnitude of increase in retinal cGMP metabolic flux determined by ^{18}O incorporation into nucleotide α-phosphoryls corresponds with intensity of photic stimulation. *Journal of Biological Chemistry*. 258:9213–9219.

Harosi, F. I. 1975. Absorption spectra and linear dichroism of some amphibian photoreceptors. *Journal of General Physiology*. 66:357–382.

Hodgkin, A. L. 1988. Modulation of ionic currents in vertebrate photoreceptors. *In* Proceedings of the Retina Research Foundation Symposium. Vol. 1. D. M. K. Lam, editor. Portfolio, The Woodlands, TX. 6–30.

Hodgkin, A. L., P. A. McNaughton, and B. J. Nunn. 1985. The ionic selectivity and calcium dependence of the light-sensitive pathway in toad rods. *Journal of Physiology*. 358:447–468.

Hodgkin, A. L., P. A. McNaughton, and B. J. Nunn. 1987. Measurement of sodium-calcium exchange in salamander rods. *Journal of Physiology*. 391:347–370.

Hodgkin, A. L., P. A. McNaughton, B. J. Nunn, and K.-W. Yau. 1984. Effect of ions on retinal rods from *Bufo marinus*. *Journal of Physiology*. 350:649–680.

Hodgkin, A. L., and B. J. Nunn. 1987. The effects of ions on sodium-calcium exchange in salamander rods. *Journal of Physiology*. 391:371–398.

Hodgkin, A. L., and B. J. Nunn. 1988. Control of light-sensitive current in salamander rods. *Journal of Physiology*. 403:439–472.

Kawamura, S., and M. Murakami. 1989. Regulation of cGMP levels by guanylate cyclase in truncated frog rod outer segments. *Journal of General Physiology*. 94:649–668.

Kilbride, P., and T. G. Ebrey. 1979. Light-initiated changes of cyclic guanosine monophosphate levels in the frog retina measured with quick-freezing techniques. *Journal of General Physiology.* 74:415–426.

Koch, K.-W., and L. Stryer. 1988. Highly cooperative feedback control of retinal rod guanylate cyclase by calcium ions. *Nature.* 334:64–66.

Korenbrot, J. I., and D. L. Miller. 1986. Calcium ions act as modulator of intracellular information flow in retinal rod phototransduction. *Neuroscience Research.* 4(Suppl):S11–S34.

Korenbrot, J. I., and D. L. Miller. 1989. Cytoplasmic free calcium concentration in dark-adapted retinal rod outer segments. *Vision Research.* 29:939–948.

Lagnado, L., L. Cervetto, and P. McNaughton. 1988. Ion transport by the Na:Ca exchange in isolated rod outer segments. *Proceedings of the National Academy of Sciences, USA.* 85:4548–4552.

Lamb, T., P. A. McNaughton, and K.-W. Yau. 1981. Spatial spread of activation and background desensitization in toad rod outer segments. *Journal of Physiology.* 319:463–486.

Liebman, P. A. 1972. Microspectrophotometry of photoreceptors. *In* Photochemistry of Vision. H. J. A. Dartnall, editor. Springer Verlag, New York. 481–528.

Lipton, S. A., H. Rasmussen, and J. E. Dowling. 1977. Electrical and adaptive properties of rod photoreceptors in *Bufo marinus.* II. Effects of cyclic nucleotides and prostaglandins. *Journal of General Physiology.* 70:771–791.

Lolley, R. N., and E. Racz. 1982. Calcium modulation of cyclic GMP synthesis in rat visual cells. *Vision Research.* 22:1481–1486.

Lühring, H., and U. B. Kaupp. 1989. Study of the mammalian cGMP-gated channels in excised membrane patches. *Biophysical Journal.* 55:377*a*. (Abstr.)

Matthews, G. 1986. Spread of the light response along the rod outer segment: an estimate from patch-clamp recordings. *Vision Research.* 26:535–541.

Matthews, H. R., R. L. W. Murphy, G. L. Fain, and T. D. Lamb. 1988. Photoreceptor light adaptation is mediated by cytoplasmic calcium concentration. *Nature.* 334:67–69.

McNaughton, P. A., L. Cervetto, and B. J. Nunn. 1986. Measurement of the intracellular free calcium concentration in salamander rods. *Nature.* 322:261–263.

Miller, D. L., and J. I. Korenbrot. 1987. Kinetics of light-dependent Ca fluxes across the plasma membrane of rod outer segments. A dynamic model of the regeneration of cytoplasmic Ca concentration. *Journal of General Physiology.* 90:397–426.

Nakatani, K., T. Tamura, and K.-W. Yau. 1990. Calcium feedback and sensitivity regulation in primate rods. *Society For Neuroscience Abstracts.* 16:465 (Abstr.)

Nakatani, K., T. Tamura, and K.-W. Yau. 1991. Light adaptation in retinal rods of the rabbit and two other non-primate mammals. *Journal of General Physiology.* 97:413–435.

Nakatani, K., and K.-W. Yau. 1988*a*. Calcium and magnesium fluxes across the plasma membrane of the toad rod outer segment. *Journal of Physiology.* 395:695–729.

Nakatani, K., and K.-W. Yau. 1988*b*. Calcium and light adaptation in retinal rods and cones. *Nature.* 334:69–71.

Nakatani, K., and K.-W. Yau. 1988*c*. Guanosine 3′:5′-cyclic monophosphate-activated conductance studied in a truncated rod outer segment of the toad. *Journal of Physiology.* 395:731–753.

Nakatani, K., and K.-W. Yau. 1989. Sodium-dependent calcium extrusion and sensitivity regulation in retinal cones of the salamander. *Journal of Physiology.* 409:525–548.

Nicol, G. D., and M. D. Bownds. 1989. Calcium regulates some, but not all, aspects of light adaptation in rod photoreceptors. *Journal of General Physiology.* 94:233–259.

Pepe, I. M., I. Panfoli, and C. Cugnoli. 1986. Guanylate cyclase in rod outer segments of the toad retina. *FEBS Letters.* 203:73–76.

Pugh, E. N., and W. H. Cobbs. 1986. Visual transduction in vertebrate rods and cones: a tale of two transmitters, calcium and cyclic GMP. *Vision Research.* 26:1613–1643.

Ratto, G. M., R. Payne, W. G. Owen, and R. Y. Tsien. 1988. The concentration of cytosolic free calcium in vertebrate rod outer segments measured with Fura-2. *Journal of Neuroscience.* 8:3240–3246.

Rispoli, G., A. T. Fineberg, and P. B. Detwiler. 1990. Null current measurements provide estimate of intracellular Ca in ROS. *Biophysical Journal.* 57:368*a*. (Abstr.)

Rispoli, G., W. A. Sather, and P. B. Detwiler. 1988. Effect of triphosphate nucleotides on the response of detached rod outer segments to low external calcium. *Biophysical Journal.* 53:388*a*. (Abstr.)

Schnapf, J. L., B. J. Nunn, M. Meister, and D. A. Baylor. 1990. Visual transduction in cones of the monkey *Macaca fascicularis*. *Journal of Physiology.* 427:681–713.

Schnetkamp, P. P. M. 1986. Sodium-calcium exchange in the outer segments of bovine rod photoreceptors. *Journal of Physiology.* 373:25–45.

Shapley, R., and C. Enroth-Cugell. 1984. Visual adaptation and retinal gain controls. *Progress in Retinal Research.* 3:263–346.

Sneyd, J., and D. Tranchina. 1989. Phototransduction in cones: an inverse problem in enzyme kinetics. *Bulletin of Mathematical Biology.* 51:749–784.

Stiles, W. A. 1959. Color vision: the approach through increment-threshold sensitivity. *Proceedings of the National Academy of Sciences, USA.* 45:100–144.

Stryer, L. 1986. Cyclic GMP cascade of vision. *Annual Review of Neuroscience.* 9:87–119.

Tamura, T., K. Nakatani, and K.-W. Yau. 1989. Light adaptation in cat retinal rods. *Science.* 245:755–758.

Torre, V., H. R. Matthews, and T. D. Lamb. 1986. Role of calcium in regulating the cyclic GMP cascade of phototransduction in retinal rods. *Proceedings of the National Academy of Sciences, USA.* 83:7109–7113.

Wikler, K. C., and P. Rakic. 1990. Distribution of photoreceptor subtypes in the retina of diurnal and nocturnal primates. *Journal of Neuroscience.* 10:3390–3401.

Yamazaki, A., I. Sen, M. W. Bitensky, J. E. Casnellie, and P. Greengard. 1980. Cyclic GMP-specific, high affinity, noncatalytic binding sites on light-phosphodiesterase. *Journal of Biological Chemistry.* 255:11619–11624.

Yau, K.-W., and D. A. Baylor. 1989. Cyclic GMP-activated conductance of retinal photoreceptor cells. *Annual Review in Neuroscience.* 12:289–327.

Yau, K.-W., L. W. Haynes, and K. Nakatani. 1986. Roles of calcium and cyclic GMP in visual transduction. *In* Membrane Control of Cellular Activity. H. Ch. Lüttgau, editor. Gustav Fischer, Stuttgart. 343–366.

Yau, K.-W., T. D. Lamb, and D. A. Baylor. 1977. Light-induced fluctuations in membrane current of single toad rod outer segments. *Nature.* 269:78–80.

Yau, K.-W., P. A. McNaughton, and A. L. Hodgkin. 1981. Effects of ions on the light-sensitive current in retinal rods. *Nature.* 292:502–505.

Yau, K.-W., and K. Nakatani. 1984*a*. Cation selectivity of light-sensitive conductance in retinal rods. *Nature.* 309:352–354.

Yau, K.-W., and K. Nakatani. 1984*b*. Electrogenic Na-Ca exchange in retinal rod outer segment. *Nature.* 311:661–663.

Yau, K.-W., and K. Nakatani. 1985*a*. Light-induced reduction of cytoplasmic free calcium in retinal rod outer segment. *Nature.* 313:579–582.

Yau, K.-W., and K. Nakatani. 1985*b*. Light-suppressible, cyclic GMP-sensitive conductance in the plasma membrane of a truncate rod outer segment. *Nature.* 317:252–255.